



**HAL**  
open science

## **Evidence of new particle formation within Etna and Stromboli volcanic plumes and its parameterization from airborne in-situ measurements**

Maher Sahyoun, Evelyn Freney, Joel Brito, Jonathan Duplissy, Mathieu Gouhier, Aurélie Colomb, Régis Dupuy, Thierry Bourianne, John Nowak, Chao Yan, et al.

### ► To cite this version:

Maher Sahyoun, Evelyn Freney, Joel Brito, Jonathan Duplissy, Mathieu Gouhier, et al.. Evidence of new particle formation within Etna and Stromboli volcanic plumes and its parameterization from airborne in-situ measurements. *Journal of Geophysical Research: Atmospheres*, inPress, 10.1029/2018JD028882 . hal-02076923

**HAL Id: hal-02076923**

**<https://hal.science/hal-02076923>**

Submitted on 27 Mar 2019

**HAL** is a multi-disciplinary open access archive for the deposit and dissemination of scientific research documents, whether they are published or not. The documents may come from teaching and research institutions in France or abroad, or from public or private research centers.

L'archive ouverte pluridisciplinaire **HAL**, est destinée au dépôt et à la diffusion de documents scientifiques de niveau recherche, publiés ou non, émanant des établissements d'enseignement et de recherche français ou étrangers, des laboratoires publics ou privés.

1 **Evidence of new particle formation within Etna and Stromboli volcanic plumes and**  
2 **its parameterization from airborne in-situ measurements**

3  
4 **Maher Sahyoun<sup>1</sup>, Evelyn Freney<sup>1</sup>, Joel Brito<sup>1,\*</sup>, Jonathan Duplissy<sup>2</sup>, Mathieu Gouhier<sup>3</sup>,**  
5 **Aurélie Colomb<sup>1</sup>, Regis Dupuy<sup>1</sup>, Thierry Bourianne<sup>4</sup>, John B. Nowak<sup>5</sup>, Chao Yan<sup>2</sup>, Tuukka**  
6 **Petäjä<sup>2</sup>, Markku Kulmala<sup>2</sup>, Alfons Schwarzenboeck<sup>1</sup>, Céline Planche<sup>1</sup>, and Karine Sellegri<sup>1</sup>**

7 <sup>1</sup> Laboratoire de Météorologie Physique INSU-CNRS UMR 6016, Université Clermont  
8 Auvergne, 63000 Clermont -Ferrand, France

9 <sup>2</sup> Institute for Atmospheric and Earth System Research/Physics, Faculty of Science, University of  
10 Helsinki, P.O. Box 64, 00014 Helsinki, Finland

11 <sup>3</sup> Laboratoire Magmas et Volcans CNRS, IRD, Observatoire de Physique du Globe de  
12 Clermont-Ferrand, Université Clermont Auvergne, 63000 Clermont -Ferrand, France

13 <sup>4</sup> Center National de Recherches Météorologiques, Météo-France, Toulouse, URA1357, France

14 <sup>5</sup> Chemistry and Dynamics Branch, NASA Langley Research Center, Hampton, VA 23681, USA

15 \* Now at IMT Lille Douai, Université Lille, SAGE, 59000 Lille, France

16  
17 Corresponding author: Karine Sellegri ([k.sellegri@opgc.univ-bpclermont.fr](mailto:k.sellegri@opgc.univ-bpclermont.fr)) and Maher Sahyoun  
18 ([maher.sahyoun@uca.fr](mailto:maher.sahyoun@uca.fr)).

19 **Key Points:**

- 20 • New particle formation was evidenced to occur within different volcanic plumes of Etna  
21 and Stromboli
- 22 • The new particle formation is more pronounced in the free troposphere than in marine  
23 boundary layer
- 24 • The growth of the newly formed particles to the CCN active size was observed to occur  
25 within the volcanic plumes in different rates
- 26 • A novel parameterization rate of new particle formation within the Etna's volcanic  
27 passive plume was proposed based on the actual measurements

28 **Abstract**

29 Volcanic emissions can significantly affect the Earth's radiation budget by emitting  
30 aerosol particles and gas-phase species that can result in the new particle formation (NPF). These  
31 particles can scatter solar radiation or modify cloud properties, with consequences on health,  
32 weather, and climate. To our knowledge, this is the first dedicated study detailing how gas-phase  
33 precursors emitted from volcanic plumes can influence the NPF. A series of airborne  
34 measurements were performed around the Etna and Stromboli volcanoes within the framework  
35 of the CLerVolc and STRAP projects. The ATR-42 aircraft was equipped with a range of  
36 instrumentation allowing the measurement of particle number concentration in diameter range  
37 above 2.5 nm, and gaseous species to investigate the aerosol dynamics and the processes  
38 governing the NPF and their growth within the volcanic plumes. We demonstrate that NPF  
39 occurs within the volcanic plumes in the Free Troposphere (FT) and Boundary Layer (BL).  
40 Typically, the NPF events were more pronounced in the FT, where the condensational sink was  
41 up to two orders of magnitude smaller and the temperature was  $\sim 20^{\circ}\text{C}$  lower than in the BL.  
42 Within the passive volcanic plume, the concentration of sulfur dioxide, sulfuric acid, and  $\text{N}_{2.5}$   
43 were as high as 92 ppbV,  $5.65 \times 10^8$  and  $2.4 \times 10^5 \text{ cm}^{-3}$ , respectively. Using these measurements,  
44 we propose a new parameterization for NPF rate ( $J_{2.5}$ ) within the passive volcanic plume in the  
45 FT. These results can be incorporated into mesoscale models to better assess the impact of the  
46 particle formed by natural processes, i.e. volcanic plumes, on climate.

47 **1 Introduction**

48 Volcanic emissions are found to be one of the most abundant natural sources of particles  
49 and gases in the atmosphere (Bobrowski et al., 2007; Boulon et al., 2011; Haywood & Boucher,  
50 2000; Oppenheimer et al., 2011; Oppenheimer et al., 2003; Robock, 2000; Tomasi & Lupi,  
51 2016). Volcanos emit a wide range of different gases ( $\text{SO}_2$ ,  $\text{CO}_2$ ,  $\text{H}_2\text{O}$ ,  $\text{H}_2\text{S}$ , HF, HBr, ...) and  
52 particle types (ash and aerosol particles formed from condensable vapors, metals) (Aiuppa et al.,  
53 2006; Bobrowski et al., 2007; Mather, 2015; Roberts et al., 2018; Simpson et al., 1999) into the  
54 atmosphere. Volcanic aerosols can scatter the solar radiation back to space contributing to a  
55 global cooling effect (direct effect) (Albrecht, 1989; Haywood & Boucher, 2000; Robock, 2000),  
56 or modify the climatic impacts of clouds (indirect effect) (Mather, 2015 and references within)  
57 by acting as cloud condensation nuclei (CCN) (Gassó, 2008; Hobbs et al., 1982; Ilyinskaya et al.,  
58 2017; Mather et al., 2003; Mather, 2015) or ice nuclei (IN) (Hoyle et al., 2011). Moreover,  
59 volcanic emissions can have significant detrimental effects on human health, the impact of which  
60 depends on aerosol physical and chemical properties (Ilyinskaya et al., 2017; Schmidt et al.,  
61 2011; Schmidt et al., 2015).

62 The two main types of volcanic aerosols present in the atmosphere are either primarily  
63 emitted or secondarily formed (Mather, 2015; Mather et al., 2003; Petäjä et al., 2012; Roberts et  
64 al., 2018; Robock, 2000). The primary volcanic aerosols are mainly volcanic ash and can have  
65 diameters ranging from very fine ash (sub-micron) to 2 mm according to classic sedimentology.  
66 The very fine ash, which survives proximal sedimentation, usually ranges from sub-micron to a  
67 few microns and they result from the fragmentation of the erupting magma into juvenile solid  
68 particles injected into a rising column and dispersed in the atmosphere (Allard et al., 2000; Rose  
69 & Durant, 2009). The secondary volcanic aerosol particles are produced from the gas-to-particle  
70 conversion (secondary formation) process, specifically from the oxidation of  $\text{SO}_2$  (Mather et al.,  
71 2004; Mather, 2015; Naughton et al., 1975; Schmidt et al., 2011), and this process is not yet well

72 characterized within the volcanic plumes. This process is called new particle formation (NPF),  
73 where clusters are formed from the gaseous phase as a first step and, later on, grow to larger  
74 sizes ( $> 100$  nm) at which they can act as CCN (Hobbs et al., 1982; Mather et al., 2003) or IN  
75 (Hoyle et al., 2011) and impact the climate (Kerminen et al., 2012; Kulmala et al., 2001, 2004,  
76 2014; Kulmala & Kerminen, 2008; Kulmala & Laaksonen, 1990; Makkonen et al., 2012). During  
77 active eruptions, both primary and secondary particles are present in different atmospheric  
78 vertical layers (Ilyinskaya et al., 2017; Mather & Pyle, 2015; Tulet et al., 2017). On the other  
79 hand, during passive emissions primary aerosols, with low concentrations, are often limited to  
80 the remobilization of accidental lithic (derived from the conduit and crater walls), while  
81 emissions of gaseous species may remain significant, likely to contribute to the formation of new  
82 particles. It is estimated that  $\sim 9$  Tg/year of  $\text{SO}_2$  is emitted from degassing passive volcanoes  
83 worldwide (Allard et al., 1991; Mather et al., 2003; Mather & Pyle, 2015; Pyle & Mather, 2003),  
84 being roughly the same order of magnitude of continuously and sporadically eruptive volcanoes  
85 (Andres & Kasgnoc, 1998; Carn et al., 2016). Currently, volcanoes contribute to  $\sim 10\%$  of the  
86 global budget of sulfur emission sources that are dominated by anthropogenic emissions (Allard  
87 et al., 1991; Smith et al., 2011). Past studies estimated that aerosol particles with diameters  
88 smaller than  $0.1 \mu\text{m}$  contributed a total of 6 to 18% to the total aerosol volume in the passive  
89 plume from Etna in Italy (Watson & Oppenheimer, 2000). Whereas in Stromboli (Italy), the  
90 contribution of particles in the nucleation and accumulation modes was estimated to be 66% of  
91 the total aerosol volume (Allard et al., 2000). Recent studies estimated that global NPF  
92 contributes up to 54% of CCN with a large uncertainty range of 38–66% in the present-day  
93 atmosphere (Gordon et al., 2017), which is higher than what has been estimated in past studies  
94 (Merikanto et al., 2009). In the preindustrial atmosphere simulations, NPF is shown to contribute  
95 up to 68% with an even larger range of uncertainty at 45–84% (Gordon et al., 2017). However, a  
96 large fraction of the uncertainty on the impact of aerosols on climate stems from the incomplete  
97 knowledge of the pre-industrial gas and aerosol concentrations and compositions (Carslaw et al.,  
98 2013; Gordon et al., 2016, 2017), therefore, further understanding of such natural processes is  
99 crucial.

100 Sulfuric acid (SA), formed from the oxidation of  $\text{SO}_2$  through different channels, is  
101 known to be a key species in NPF processes (Kroll et al., 2015; Mauldin et al., 2003; Petäjä et  
102 al., 2011; Sipilä et al., 2010; Weber et al., 1996; Weber et al., 2003). Under certain conditions  
103 and during mildly eruptive or non-eruptive activity, SA has been observed to be already  
104 primarily emitted or secondarily formed in large quantities at some volcanoes (Ilyinskaya et al.,  
105 2012; Naughton et al., 1975; Zelenski et al., 2015). Furthermore, the formation of SA and the  
106 variation in its concentration in the atmosphere depend strongly on the abundance of  $\text{SO}_2$  and the  
107 oxidative capacity in the atmosphere (Ilyinskaya et al., 2017; Kroll et al., 2015; Mather, 2015;  
108 Schmidt et al., 2012).

109 While a large number of studies have investigated volcanic emissions through in-situ  
110 ground-based and satellite/radar measurements (Carn et al., 2013; Galle et al., 2010; Kantzas &  
111 McGonigle, 2008; Mather, 2015; McCormick et al., 2016; McGonigle & Oppenheimer, 2003;  
112 McGonigle et al., 2017), airborne in-situ measurements of volcanic emissions remain very scarce  
113 (Mauldin et al., 2003; Oppenheimer et al., 2010; Petäjä et al., 2012; Radke, 1982; Rose et al.,  
114 2006; Tulet et al., 2017; Vignelles et al., 2016; Weber et al., 2012). The limited number of  
115 volcanic plume airborne observations investigating NPF arises from challenges associated with  
116 restricted timescales and the impact of temporal and spatial plume's heterogeneities under

117 typically harsh environments, besides the costly deployment of highly sophisticated  
118 instrumentation aboard an aircraft in such harsh conditions (Delmelle, 2003; Mauldin et al.,  
119 2003; Oppenheimer et al., 2003). In that context, the aim of this study is to investigate the  
120 aerosol dynamics and the processes governing aerosol formation and growth in different types of  
121 volcanic plumes. To the best of our knowledge, this is the first comprehensive dedicated study  
122 investigating how gas-phase precursors influence NPF events within different volcanic plumes  
123 over Etna and Stromboli using airborne measurements' platforms. Such investigation allows us  
124 to characterize the plume spatial extent, its properties, and its intensity and to derive a new  
125 parameterization of the rate of NPF. These will permit to further improving the estimation of  
126 NPF from natural sources, i.e. volcanic degassing plumes, in models to evaluate more accurately  
127 the impact of those particles on climate.

## 128 **2 Methodology and measurements conditions**

### 129 2.1 The volcanoes

130 The airborne measurements were conducted around the Etna and Stromboli volcanoes  
131 (Italy). Etna is located on the East coast of Sicily in the Mediterranean Sea (37.75° N, 14.99° E).  
132 The vent is located at 3330 m above sea level (a.s.l), typically in the free troposphere (FT).  
133 Mount Etna exhibits basaltic eruptions ranging from weakly explosive low-volume activity, such  
134 as Stromboli, to more powerful explosive activity leading to fire fountains, which feed columns  
135 of scoria, bombs, and ash as jets to heights of tens to hundreds of meters (Calvari et al., 2011).  
136 Occasionally, Mount Etna exhibits even more powerful eruptions and produces sub-plinian  
137 plumes injecting large amounts of ash and gas, although limited to the troposphere. Inter-  
138 eruptive periods are usually characterized by significant emissions of gas, making Etna volcano  
139 one of the most important SO<sub>2</sub> emitter (Calvari et al., 2011). During the eruptive activity, the  
140 average flux of SO<sub>2</sub> emitted at Etna is typically in the range 10-25 kt/day (Caltabiano et al.,  
141 1994), and decreases to 0.6-2 kt/day (Aiuppa et al., 2008; Roberts et al., 2018) during passive  
142 emissions. Stromboli is one of the Aeolian Islands in the Mediterranean Sea located in the north  
143 coast of Sicily (38.79°N, 15.21°E) and the vent is at 924 m a.s.l., estimated to be in the boundary  
144 layer (BL) during our measurements in summer daytime (Seidel et al., 2012). Stromboli volcano  
145 is known to exhibit short-lived low-explosive activity with explosions occurring at a time  
146 interval of a few tens of minutes on average (Blackburn et al., 1976). The average flux of SO<sub>2</sub>  
147 emitted during a standard level of activity lies in the range 0.15-0.6 kt/day (Burton et al., 2008).

148 During the time of our campaign, Etna was not erupting and only products of passive  
149 emissions could be recorded. On the contrary, at Stromboli volcano, the Northeast craters  
150 exhibited the typical Strombolian activity with small gas bursts accompanied by the ejection of  
151 ballistics every 5-10 min, while the Southwest crater produced less frequent ash-rich explosions.  
152 The threshold of the SO<sub>2</sub> flux rate is up to ~5000 t/day for Etna volcano and ~200-300 t/day for  
153 Stromboli volcano as reported by the National Institute of Geophysics and Volcanology in Italy  
154 for the week between 13 and 20 June 2016, Report. N° 25/2016 on the 21<sup>st</sup> of June 2016  
155 (National Institute of Geophysics and Volcanology, 2016 a; b).

### 156 2.2 Research flights

157 In 2016, as part of the CLerVolc and STRAP projects (Centre Clermontois de Recherche  
158 sur le Volcanisme and Trans-disciplinary collaboration to investigate volcano plumes risks), a  
159 series of airborne-based (French research aircraft, ATR-42) measurements were performed

160 around Etna and Stromboli volcanoes on the 15<sup>th</sup> and 16<sup>th</sup> of June 2016. The ATR-42, operated  
161 by the French SAFIRE Facility (Service des Avions Français Instrumentés pour la Recherche en  
162 Environnement), intercepted the volcanic plume close to the vent (~2.5 to 5 km) and tracked its  
163 evolution for up to 120 km. During this campaign, four flights were conducted: two around Etna  
164 (called herein ETNA13 and ETNA14) and two around the Stromboli (called herein STRO14 and  
165 STRO15) (Table 1).

**Table 1: Summary of ATR-42 flight during STRAP campaign over Etna and Stromboli volcanoes. The date, taking-off and landing time (UTC, UTC=local time -2h) and the maximum and minimum of the longitude, latitude, altitude and the corresponding pressure reached during the flights**

Date	Flight name and number	Take-off – landing time (UTC)	Latitude range	Longitude range	Altitude range (m) Pressure (hPa) <i>FT or BL</i>
15-Jun-2016	ETNA13	10:43:04 – 11:17:49	37.651 – 37.868	14.969 – 15.515	1917-3625 810-659.6 <i>FT</i>
15-Jun-2016	ETNA14	14:08:08 – 14:59:58	37.593 – 37.820	15.079 – 15.905	1966-3195 805.3-696 <i>FT</i>
15-Jun-2016	STRO14	15:19:53 – 15:54:53	38.652 – 38.852	15.183 – 15.637	715-955 929.6-904.6 <i>BL</i>
16-Jun-2016	STRO15	07:38:43 – 08:59:58	38.619 – 39.904	14.408 – 15.449	68-786 997.8-921.2 <i>BL</i>

### 166 2.3 Airborne instrumentations

167 The characterization of the aerosols and gases in the volcanic plumes involved installing  
168 a number of instruments in the ATR-42, including: 1) an ultrafine water based Condensation  
169 Particle Counters (CPC) (TSI 3788) (Kupc et al., 2013) to measure the total number of particle  
170 concentration at a cut-off size > 2.5 nm in diameter; 2) the COndensation PArticle System  
171 (COPAS) CPC (Weigel et al., 2009), which is specifically dedicated to aircraft measurements, to  
172 measure particles number concentration at size cut-off > 10 nm in diameter; 3) an Optical  
173 Particle Counter (Sky OPC, Grimm, # 1.129) to measure the particle size distribution and  
174 number concentration in each size bin in the range distributed between 250 nm and 2.5 µm.  
175 According to the works of Pirjola et al. (1999), the OPC data in that size range was used to  
176 calculate the condensational sink (CS), thus, it represents the lower limit of CS calculated for this  
177 study. 4) a UV Fluorescence SO<sub>2</sub> Analyzer Teledyne API (T100 V) to measure the SO<sub>2</sub>  
178 concentration with 10 s time resolution; 5) a newly designed ambient ionization inlet (AI)  
179 coupled with the Atmospheric Pressure interface – Time Of Flight (AI-APi-ToF) mass  
180 spectrometer (MS), developed at Institute for Atmospheric and Earth System Research of the  
181 University of Helsinki (Finland) (Junninen et al., 2010), to measure SA concentration (more  
182 details about SA calibration is further given in section 2.4).

183 This combination of different instruments, all having a time resolution of 1s, covered a  
184 wide particle size range (2.5 nm up to ~ 2500 nm in diameter) allowing the measurements of  
185 aerosol physical properties and the detection of both nanoparticle nucleation and growth  
186 processes. The variables defined from the in-situ measurements of total particle number  
187 concentrations ( $\text{cm}^{-3}$ ) together with the SA and  $\text{SO}_2$  are summarized in Table 2.

*Table 2: Summary of the variables and corresponding instrumentations used during Etna and Stromboli flights on the 15<sup>th</sup> and 16<sup>th</sup> of June 2016.*

Variable	Name	Unit	Instrument/calculation method	Reference
Total number concentration for particles (N) at diameter > 2.5 nm	$N_{2.5}$	$\text{cm}^{-3}$	Water CPC (TSI 3788)	(Kupc et al., 2013)
N at diameter > 10 nm	$N_{10}$	$\text{cm}^{-3}$	CPC	(Weigel et al., 2009)
N at diameter > 250 nm	$N_{250}$	$\text{cm}^{-3}$	Sky OPC GRIMM, # 1.129	Manual (GRIMM, 2008)
N at diameter range between 2.5 and 10 nm	$N_{2.5-10}$	$\text{cm}^{-3}$	$N_{2.5} - N_{10}$	Derived in this study
N between 10 and 250 nm	$N_{10-250}$	$\text{cm}^{-3}$	$N_{10} - N_{250}$	Derived in this study
Sulfuric acid concentration	SA	$\text{cm}^{-3}$	CI-API-ToF	(Junninen et al., 2010)
Sulfur dioxide mixing ratio	$\text{SO}_2$	ppbV	UV Fluorescence Analyzer Teledyne API	Manual (Model T100U 2011)

188 Different meteorological variables, such as temperature (T); relative humidity (RH); wind  
189 speed (W); dew point temperature; pressure; and turbulence, were also measured aboard the  
190 aircraft with a one second time resolution. The statistics and the variation range of the T, RH,  
191 and W are shown in Table 3. The time series of the abovementioned meteorological parameters  
192 are displayed in Figure S1 (supplementary information) for each flight.

193

*Table 3: Summary of the thermodynamic parameters of the atmosphere measured for the different flights. 10<sup>th</sup> and 90<sup>th</sup> percentile are given in the square brackets and the median values are given in the second line.*

Variable	ETNA13	ETNA14	STRO14	STRO15
T ( $^{\circ}\text{C}$ )	[7.4 - 14.4] 10.45	[11.5 - 14.7] 12.5	[22.9 - 24] 23.5	[29.4 - 31.9] 30.9
RH (%)	[35.2 - 72.6] 61.5	[34.2 - 53.3] 42.6	[27.6 - 42.5] 39	[27.6 - 36] 30.4
W ( $\text{m s}^{-1}$ )	[10.1 - 21.6] 18.2	[9 - 19] 15.8	[3.8 - 6.6] 5.2	[13.5 - 24.5] 17.9

194 For flights ETNA13 and ETNA14 that took place in the FT, the temperature was above 5  $^{\circ}\text{C}$ ,  
195 reaching a maximum of 17.5  $^{\circ}\text{C}$  at ~ 2 km in altitude. In STRO14 and STRO15 that took place in  
196 the BL, the temperature was always detected over 20 $^{\circ}\text{C}$  at lower altitudes and it was 10 to 20 $^{\circ}\text{C}$   
197 higher than the temperatures observed in the FT. The RH did not exceed 62.5% and 82% for  
198 flights ETNA13 and ETNA14 and it was even lower in the Stromboli plumes (Figure S.1 and  
199 Table 3). The measurements of the cloud droplet probe (CDP) and fast cloud droplet probe

200 (FCDP) together with the RH measurements confirm that flights were undertaken in cloud-free  
201 conditions.

#### 202 2.4 SA calibration from AI-API-ToF

203 Following the strict aircraft instrumentation regulation concerning chemicals, a new  
204 ambient ionization (AI) inlet has been developed for the field campaign avoiding the use of  
205 chemical reagents. The AI-API-ToF is used for the first time on board an aircraft to perform such  
206 measurements and provides a 1 s time resolution of a lower estimate of SA concentration. The  
207 system utilizes a soft X-ray source (Hamamatsu L9490) to ionize directly the sampled air and  
208 increase the overall signal for fast (1 s) measurement. The instrument was also operated in ion  
209 mode, like a classical API-ToF MS mode, where only natural ions are sampled. However, in the  
210 ion mode, a long integration time (minimum 10 min) is necessary to obtain the correct signal.  
211 The X-ray source was periodically switched ON and OFF (for these flights, 10 seconds ON and  
212 10 seconds OFF), allowing both sampling of natural ions and forced ionized ions. The ATR-42  
213 was flying at an average speed of 360 km/hour; hence, we use the X-ray mode (with one-second  
214 resolution) to first identify the different air masses (i.e. inside the plume, outside the plume) and  
215 in a second step to analyze the average natural ions spectrum within the volcanic plume. After  
216 the flight campaign, a calibration campaign took place during CLOUD11 at the CLOUD  
217 chamber similarly to previous CLOUD experiments (Kirkby et al., 2011; Rondo et al., 2016). In  
218 the CLOUD chamber, various atmospheric systems were studied with a wide range of species,  
219 i.e. SO<sub>2</sub> (0ppb - 2.6ppb), NO<sub>x</sub> (0ppb - 33ppb) and organic vapors (alpha-pinene (0ppb - 4.5ppb),  
220 isoprene (0ppb - 5ppb), trimethyl-benzene (0ppb - 9ppb)), allowing the characterization of the  
221 new flying AI in different atmospheric systems. During this calibration campaign, the new flying  
222 AI inlet worked mainly in O<sub>2</sub><sup>-</sup> chemical ionization modes, however, when NO<sub>x</sub> was at high  
223 concentrations in the chamber, NO<sub>3</sub><sup>-</sup> ionization could also contribute. Estimates of SA  
224 concentration are conducted from the signal that is produced from the ionization of O<sub>2</sub><sup>-</sup> ions  
225 (HSO<sub>4</sub><sup>-</sup>) and NO<sub>3</sub><sup>-</sup> (H<sub>2</sub>SO<sub>4</sub> NO<sub>3</sub>), obtaining a good correlation between well-characterized nitrate  
226 API-ToF MS systems and the instrument used here (supplementary Figure S.3).

227

#### 228 2.5 Backward trajectories

229 The 72 h air mass backward trajectories were calculated first at the vent of the volcano at  
230 the beginning of the flight and then at the flight track every 10 minutes along the path of each  
231 flight trajectory using the HYSPLIT model (Draxler, 2003; Stein et al., 2016) (Figure S2).  
232 According to back-trajectory calculations, the air mass that reached Etna originated mostly from  
233 the Atlantic Ocean passing through Spain and the Mediterranean Sea. Similar back-trajectory  
234 was observed for STRO14, however, STRO15 back-trajectory suggests an origin crossing above  
235 the Saharan desert. During the latter event, a significant aerosol surface area in the background  
236 was observed and could be explained by the presence of Saharan dust, in contrast to the other  
237 three flights.

#### 238 2.6 Background and plume conditions

239 We measured the SO<sub>2</sub> concentration over the Mediterranean in both the FT and BL  
240 outside of the volcanic plumes of Etna and Stromboli and the values were ranging from 1.4 to  
241 1.9 ppbV. From the air mass characterization upwind and downwind of Etna (being almost all

242 the time in the FT) and Stromboli (in the BL), a background plume threshold value (PTV) of 2  
243 ppbV of SO<sub>2</sub> is used. This threshold value is used to exclude any contributions from ship  
244 emissions or other anthropogenic sources, etc. Although the PTV could be considered relatively  
245 high when compared to anthropogenic emission levels (usually on average below 1 ppbV) or to  
246 other studies (Mauldin et al., 2003), these values were chosen to ensure that our data analysis  
247 focused only on measurements within the different volcanic plumes, and to ensure that we do not  
248 consider contributions from other sources. The background (outside plume conditions) was also  
249 characterized in term of particle concentrations, being defined as median of all the measures  
250 (defined in Table 2) when SO<sub>2</sub> < 2 ppbV for Etna (i.e. 1.61 ppbV, 1781 cm<sup>-3</sup>, 3.2 cm<sup>-3</sup> and  
251 0.85×10<sup>8</sup> cm<sup>-3</sup> for SO<sub>2</sub>, N<sub>2.5</sub>, N<sub>250</sub> and SA, respectively) and Stromboli (i.e. 1.26 ppbV, 2100 cm<sup>-3</sup>  
252 <sup>3</sup>, 10.75 cm<sup>-3</sup> and 0.87×10<sup>8</sup> cm<sup>-3</sup> for SO<sub>2</sub>, N<sub>2.5</sub>, N<sub>250</sub> and SA, respectively). The SO<sub>2</sub>, SA, and  
253 particle number concentrations were corrected considering that their backgrounds were  
254 subtracted from the plume concentrations in order to quantify the volcanic plume increment.  
255 Thus, all the analysis presented in the following sections is under plume conditions.

### 256 3 Results and discussion

#### 257 3.1 Plume spatial extent and total particle number concentrations

258 The spatial extent (vertical and horizontal) of the different volcanic plumes, represented by the  
259 SO<sub>2</sub>, is displayed in Figure 1. Once the aircraft arrived at the volcano, a total vertical profile  
260 ranging from 0.2 km up to 4 km for both plumes (Figure 1) was performed. The Etna plume  
261 appeared to be located at altitudes between 2 and 3.6 km, whereas the Stromboli plume was  
262 centered around 0.8 km during STRO14 and as low as 0.2 km during STRO15. We, therefore,  
263 assume that both volcanic plumes investigated around Stromboli were in the BL Once the plume  
264 vertical distribution was located, a series of horizontal transects took place up to distances of 120  
265 km.

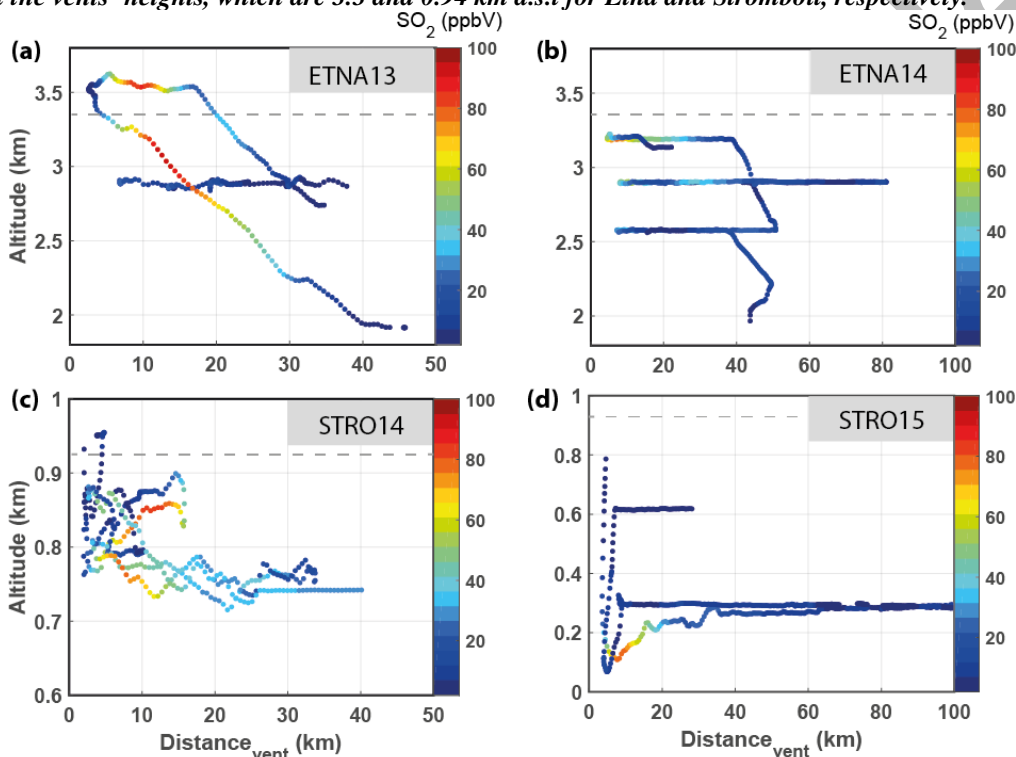
266 For ETNA13 and ETNA14 and within the plume conditions, the vertical sounding shows  
267 that the air mass containing the plume moved towards downwind above 2 km in altitude  
268 confirming the presence of the plume in the FT. The median SO<sub>2</sub> concentrations were 13.7 and  
269 13.55 ppbV and reached maximum values at 92.3 and ~ 77 ppbV for ETNA13 and ETNA14,  
270 respectively. Since we did not sample the exact center of the plume at the vent where SO<sub>2</sub> should  
271 peak, the maximum of SO<sub>2</sub> was observed at altitudes above 3 and ~2.8 km at ~ 13 and 10 km  
272 away from the vent for ETNA 13 and 14, respectively (Figure 1; a-b). Subsequently, SO<sub>2</sub>  
273 concentrations decreased with distance from the vent and decreased in altitude while travels  
274 downwind below 2.8 km (Figure 1; a-b). The plume can still be observed above the altitude of  
275 2.8 km with relatively high SO<sub>2</sub> values above 40 ppbV at ~22 km distant from the vent (Figure 1;  
276 a-b).

277 For STRO14 and STRO15 in BL, the SO<sub>2</sub> median concentrations were 28.33 and 7.3  
278 ppbV and reached the maxima of 83.3 and 78.3 ppbV, respectively (Figure 1; c-d). The median  
279 concentration of SO<sub>2</sub> observed in STRO15 is a factor of ~2 less than what was observed in both  
280 cases in the FT whereas, in STRO14, the median was a factor of ~2 larger than in the FT. The  
281 differences in the median concentrations of the two BL flights can be explained by the relatively  
282 low wind speed measured in the case of STRO14 compared to the other flights (Table 3),  
283 resulting in the plume being less spread in both horizontal and vertical directions and more  
284 concentrated over a shorter range of distance (Figure 1). Since the aircraft missed the core of the  
285 plume at the vent, the maximum values were observed at distances ~ 10 to 12 km from the vent

286 similarly to Etna plumes and at height of 860 and 120 m (Figure 1; c-d), respectively, indicating  
287 a downward transport of the plume. The SO<sub>2</sub> concentration decreases significantly (< 15 ppbV)  
288 (Figure 1; d) with distance from the vent.

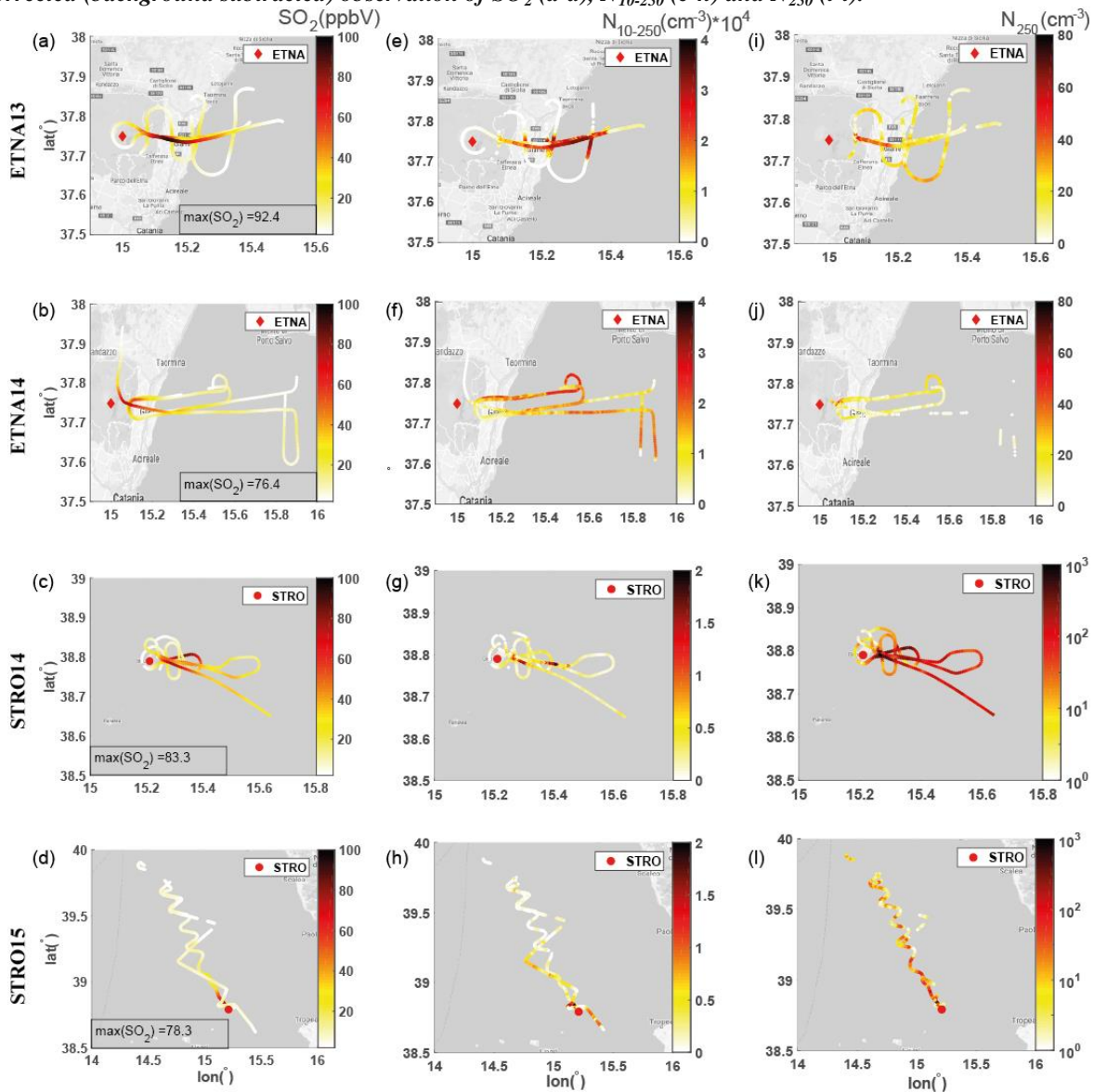
289 The concentration of SO<sub>2</sub> measured during all flights is on the same order of magnitude  
290 as those observed in previously reported airborne measurement (larger than 10 ppbV) over the  
291 Miyaka volcano in the Pacific Ocean in Japan (Mauldin et al., 2003).

**Figure1: The plume spatial extent represented by the concentration of SO<sub>2</sub> as a function of altitudes and distance from the volcanic vent for a) ETNA13, b) ETNA14, c) STRO14 and d) STRO15. The dashed lines represent the vents' heights, which are 3.3 and 0.94 km a.s.l for Etna and Stromboli, respectively.**



292 The maps of the aircraft trajectories for the four flights are shown in Figure 2, where the  
293 color bar represents the concentration of SO<sub>2</sub>, N<sub>10-250</sub>, and N<sub>250</sub>. In the FT, N<sub>10-250</sub> increased along  
294 the plume with median concentrations of ~2500 and 14000 cm<sup>-3</sup> for ETNA13 and ETNA14,  
295 respectively (Table 4). The maximum concentrations of N<sub>10-250</sub> were measured to be 34100 cm<sup>-3</sup>  
296 and 25400 cm<sup>-3</sup> at ~26 and ~47 km distant from the vent. Thus, the N<sub>10-250</sub> maxima positions  
297 were at ~13 and 37 km farther than the areas where SO<sub>2</sub> maxima were detected (Figure 2; a-b  
298 and e-f). The N<sub>10-250</sub> increases, on average, from few thousands at ~5 km to few ten thousand  
299 at distance > 25 km from the vent, for Etna flights (Figure 2; e-f) and the rate of this increase  
300 roughly was ~1500 cm<sup>-3</sup> per km. This suggests the occurrence of new particle formation and  
301 growth along the volcanic plume. For larger particles, the median of N<sub>250</sub> were 18.8 cm<sup>-3</sup> and 11  
302 cm<sup>-3</sup> for flights ETNA13 and ETNA14, respectively (Table 4). During ETNA flights, the N<sub>250</sub>  
303 was relatively high (~70 cm<sup>-3</sup>) close to the vent (~7 km), but decreased significantly (< 20 cm<sup>-3</sup>)  
304 with the plume dilution (Figure 2; i-j and Figure S4). This is opposite to what was measured for  
305 smaller particles (N<sub>10-250</sub>) where a higher concentration was detected along the volcanic plume in  
306 the FT especially in the diluted plume (> 25 km) of both Etna flights (Figure 2; e-f).

**Figure 2: Maps of the trajectory of the different flights in the FT and BL. The color-coded bars represent the corrected (background subtracted) observation of  $SO_2$  (a-d),  $N_{10-250}$  (e-h) and  $N_{250}$  (i-l).**



307 Considering that the volcanic emissions in ETNA13 and ETNA14 during the time of the  
 308 campaign were passive, the presence of large particles can mainly be interpreted as the rapid  
 309 growth of freshly nucleated particles. This hypothesis is confirmed by the correlation between  
 310  $N_{100}$ ,  $N_{250}$ , and  $N_{10}$  (Figure S5; a, c). We do not exclude that some fraction of these particles may  
 311 also be due to the presence of very fine primary particles (accidental lithic) remobilized from the  
 312 previous deposits within the conduit and volcanic crater walls, but we estimate that their  
 313 contribution to the total aerosol concentration was minimal in our observation in the FT (Figure  
 314 S5; a, c).

315 For STRO14 and STRO15,  $N_{10-250}$  was observed with relatively large values ( $> 10^4 \text{ cm}^{-3}$ )  
 316 close to the vent at  $\sim 4 \text{ km}$ , respectively, and then decreased significantly with distance from the  
 317 vent (Figure 2; g-h), except the area where  $N_{10-250}$  peaks at  $\sim 12 \text{ km}$  distant from the vent for  
 318 STRO14 (Figure 2; g). The  $N_{10-250}$  maxima were  $18809 \text{ cm}^{-3}$  and  $19700 \text{ cm}^{-3}$  at  $\sim 12 \text{ km}$  and  $\sim 7$   
 319  $\text{km}$  for STRO14 and STRO15, respectively, where  $SO_2$  was also observed to be relatively large

320 (> 60 ppbV). This is in contrast to what we observed for Etna plumes, where the  $N_{10-250}$  maxima  
321 were located farther downwind (i.e. at 26 and 47 km distant from the vent. The median of  $N_{10-250}$   
322 concentrations were  $2470 \text{ cm}^{-3}$  and  $1300 \text{ cm}^{-3}$  for both Stromboli flights, i.e. close to the  $N_{10-250}$   
323 median concentration measured within the ETNA13 but one order of magnitude less than the  
324 median  $N_{10-250}$  observed for ETNA14.

**Table 4: Summary of the number concentrations ( $\text{cm}^{-3}$ ) of particles at different diameter ranges, SA concentration and the CS rate ( $\text{s}^{-1}$ ) measured during the different flights. 25<sup>th</sup> and 75<sup>th</sup> percentiles are in the first line in square brackets and medians are in the second line.**

VARIABLE	ETNA13	ETNA14	Stro14	Stro15
$N_{2.5-10} (\text{cm}^{-3})$	[0.99 2.4]* $10^4$ 4.2* $10^3$	[0.41 1.1]* $10^5$ 7.7* $10^4$	[0.4 1.3] * $10^3$ 638.5	[171 741] 351
$N_{10-250} (\text{cm}^{-3})$	[0.053 1.9]* $10^4$ 2.51* $10^3$	[0.7 1.81]* $10^4$ 1.4* $10^4$	[1.1 3.7]* $10^3$ 2.47* $10^3$	[428 3.1* $10^3$ ] 1.3* $10^3$
$N_{250} (\text{cm}^{-3})$	[11.2 27.6] 18.8	[5.4 16.8] 11	[16.6 150.5] 68.2	[2.5 72.5] 35
SA ( $\text{cm}^{-3}$ )	[0.85 3.9]* $10^8$ 2.9* $10^8$	[3.35 3.94]* $10^8$ 3.71* $10^8$	[2.34 2.94]* $10^8$ 2.67* $10^8$	[3 3.5]* $10^8$ 3.3* $10^8$
SO <sub>2</sub> (ppbV)	[6.2 25] 13.7	[7.5 21.6] 13.55	[13 37.6] 28.3	[4.5 9.6] 7.3
CS ( $\text{s}^{-1}$ )	[0.5 3.1]* $10^{-4}$ 1.6* $10^{-4}$	[0 2.3 ]* $10^{-4}$ 6* $10^{-5}$	[0.65 9.8]* $10^{-3}$ 4.2* $10^{-3}$	[0 4.5]* $10^{-3}$ 8.1* $10^{-4}$

325 For BL flights, the  $N_{250}$  is observed to be high peaking at 1081 and  $718.5 \text{ cm}^{-3}$  near the vent <sup>3</sup> at ~  
326 7 and 5.2 km and continue possessing high values downwind along the plume dilution reaching  
327  $225 \text{ cm}^{-3}$  at 23 km distant from the vent (Figure 2; c-d and k-l). In general, the  $N_{250}$  in the BL  
328 was observed to be higher than in the FT; the medians are factor of 3 to 6 higher in the FT (Table  
329 4) and the absolute values are two orders of magnitude higher close to the vent and all along the  
330 plume dilution (Figure 2; i-l). The presence of those large particles in the BL flights is due to the  
331 quick growth of newly formed particles at distances less than 10 km close to the vent (Figure S5;  
332 b, d blue points marked by a blue circle) and distant from the vent with a different growth rate  
333 (Figure S5; b, d light blue to red points marked by a red circle). Besides, close to the vent in  
334 STRO14, there is likely a contribution from very fine juvenile ash ejected during the short  
335 explosions at Stromboli (Figure S5; b, d; blue points marked by a green circle), which can be a  
336 significant contribution to the total aerosol surface area. Moreover, in STRO15 and based on the  
337 backward trajectory analysis, there may also be a contribution from the Saharan dust particles  
338 that arrive from North Africa to the measured areas (Figure S2). Due to the lack of aerosol  
339 composition measurements, we are unable to accurately quantify these contributions. The higher  
340 concentrations of large particles during BL flights would eventually contribute to a larger aerosol  
341 surface area along the volcanic plumes compared to FT flights within Etna's volcanic plumes.

342 In the following section, we will investigate the NPF and their potential growth processes  
343 occurring within these two different volcanic plumes.

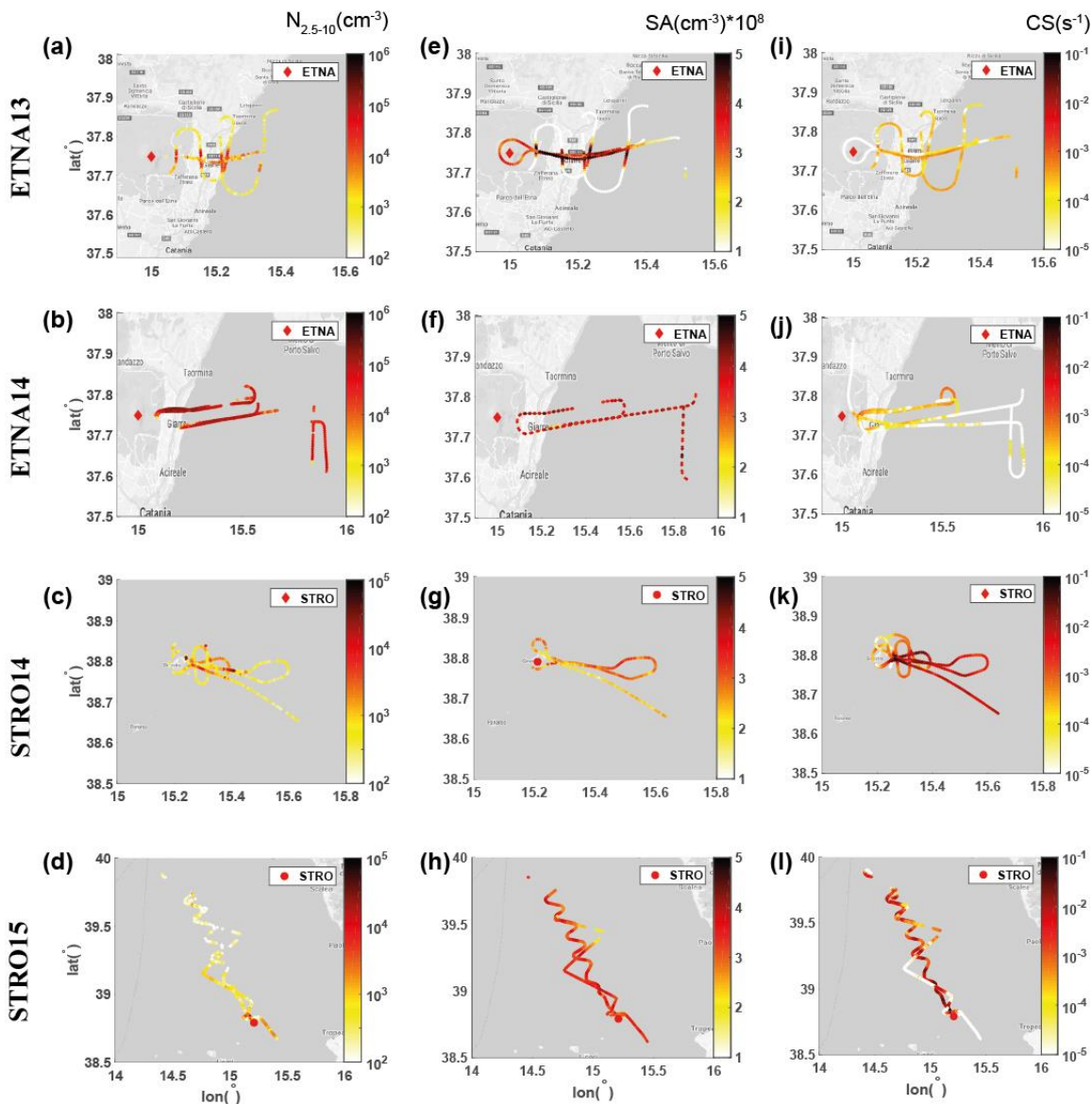
### 3.2 Observation of new particle formation within different volcanic plumes

The total number concentrations of particles between 2.5 nm and 10 nm ( $N_{2.5-10}$ ), the SA concentrations (defined in Table 2) and CS are illustrated in Figure 3. For FT flights,  $N_{2.5-10}$  concentrations were observed above the detection limit throughout both plumes and up to ~45 km away from the vent. For both Etna flights, the  $N_{2.5-10}$  is a factor of ~2 to 10 larger than the  $N_{10-250}$  concentrations. This suggests that nucleation is taking place within the volcanic passive plume in the FT (Figure 2; e-f, and Figure 3; a-b). Linked to this nucleation process occurring along the volcanic passive plume, a high concentration of SA ( $> 10^8 \text{ cm}^{-3}$ ) is continuously observed; being produced from the oxidation of  $\text{SO}_2$  (Figure 3; e-f). The maximum of  $N_{2.5-10}$  was observed where the SA concentration was greater than  $2 \times 10^8 \text{ cm}^{-3}$ , and the CS was minimum (Figure 3; a-b, e-f, i-j).

During BL flights, NPF was also observed, but high concentrations of  $N_{2.5-10}$  were mostly located close to the vent ( $< 10 \text{ km}$ ). However, the median concentration of  $N_{2.5-10}$  was up to 2 orders of magnitude less than in the FT flights. These show the evidence that new particles were formed within the different volcanic plumes close to the vent ( $\sim 3 \text{ km}$ ) for both Etna and Stromboli volcanic plumes with different rates, but also far from the vent ( $> 35 \text{ km}$ ) along the dilution of the passive plume from Etna in the FT. The higher concentrations of large particles ( $> 250 \text{ nm}$ ) in the BL result in a higher CS than in the FT (Figure 1; i-l, Figure 2; i-l, and Figure S4 and S5). Interestingly, the concentration of  $\text{SO}_2$  and SA were observed to be in comparable ranges for both volcanic plumes (Figures 1, 2; a-d and 3; e-h), and therefore do not explain solely the differences in magnitude in NPF between the FT and BL. Therefore, the greater CS together with the higher temperature, observed in the BL flights than in the FT flights, are likely to explain the weaker NPF events within the volcanic plumes in the BL (Table 2 and 4, Figure 3, and Figure S1).

Moreover, the growth behavior of the newly formed particles was distinct between ETNA and STRO plumes (Figure S4 and S5). The Correlations between newly formed particles and larger particles are observed along the volcanic plumes in both the FT and the BL (Figure S4 and S5). The growth rate, represented by the different slopes, varied according to the distance from the vent and the  $\text{SO}_2$  abundance (Figure S4 and S5). The growth is observed to increase at areas closer to the vent ( $< 20 \text{ km}$ ) than at farther areas than 20 km (Figure S4 and S5). Since SA was abundant during all flights (Figure 3; e-h), it likely played a key role in NPF and growth processes (CCN active size) within the volcanic plumes in FT and BL. It should be stressed that in the absence of the chemical analysis of the grown particles in our observation, we do not exclude the contribution of other condensable vapors to the growth of the freshly formed particles in the volcanic plumes. The growth of the newly formed particles to CCN active diameters illustrates that those particles within the volcanic plumes can contribute to cloud formation, thus, impacting the weather and climate. Such an observation might be useful for further modeling studies to investigate the contribution of NPF to the CCN and their impact on climate and reduce the associated uncertainty.

**Figure 3: Observed  $N_{2.5-10}$  (a-d), SA (e-h) and CS (i-l) along the flight trajectory within the plumes of Etna and Stromboli. Gaps visible in the different trajectories are attributed to instrumental data nonavailability.**

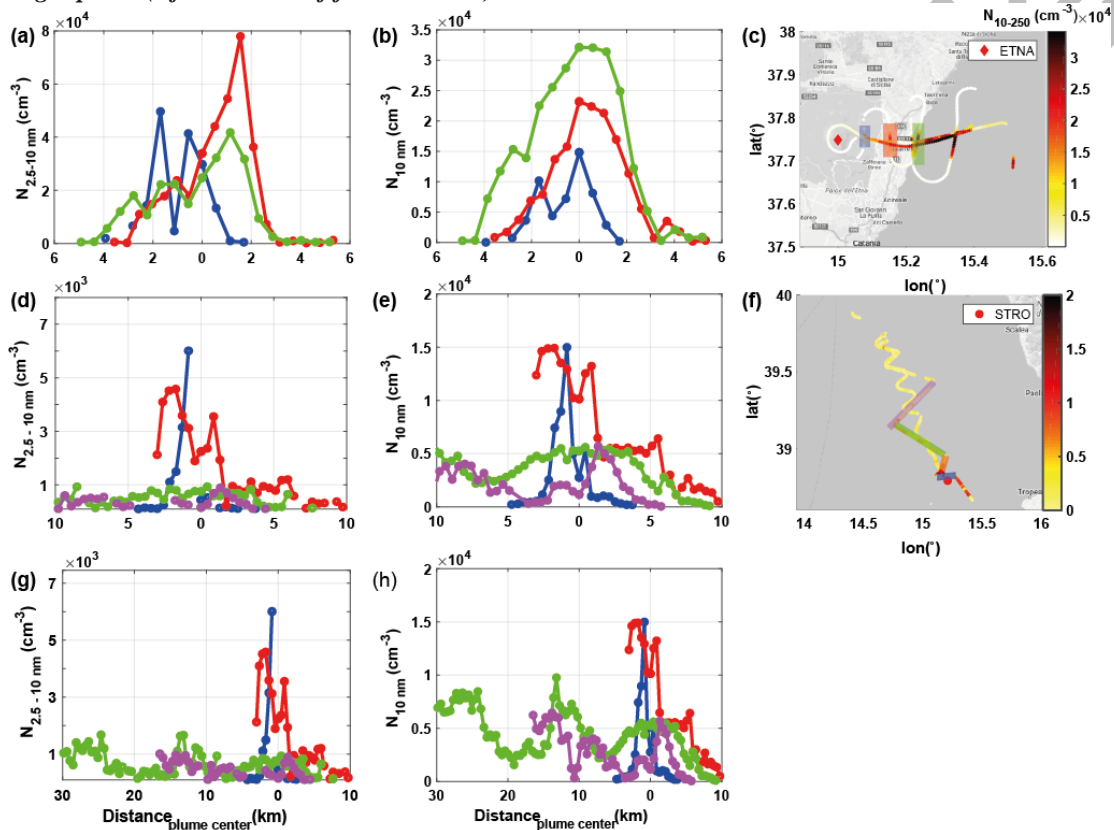


383 The volcanic SA was also observed to be abundant in other volcanic plumes of Etna  
 384 (Roberts et al., 2018) and in other locations, i.e. Miyaka and Kilauea (Kroll et al., 2015; Mauldin  
 385 et al., 2003). This abundance was found to be variable according to several factors related to SO<sub>2</sub>  
 386 concentrations and its oxidation rates, meteorological variables, i.e. wind speed, temperature and  
 387 relative humidity (Kroll et al., 2015; Roberts et al., 2018). In comparison to other studies, the SA  
 388 observed within ETNA and STRO flights were almost of the same order of magnitude to what  
 389 has been reported in the Pacific BL volcanic plume from the Miyaka volcano (Mauldin et al.,  
 390 2003; Weber et al., 2003). On the other hand, the median of N<sub>2.5-10</sub> measured in Stromboli  
 391 plumes in MBL is almost one order of magnitude larger than the upper limit (100 cm<sup>-3</sup>) reported  
 392 in the MBL volcanic plume in the Pacific from Miyaka volcano for the similar size range (3-4  
 393 and 3-8 nm) (Mauldin et al., 2003). The presence of large aerosol surface area may explain our  
 394 observation of relatively low N<sub>2.5-10</sub> in the BL, in comparison to N<sub>2.5-10</sub> observed in the FT.  
 395 Similarly, in the Pacific BL volcanic plume from Miyaka volcano (Mauldin et al., 2003), the

396 presence of pre-existing particles is given by the authors as an explanation of the low  $N_{3-4}$  and  
397  $N_{3-8}$  concentrations.

398 The spatial distributions of the plumes were analyzed in more details, through plume  
399 latitudinal transects at different distances from the vent in both ETNA13 and STRO15 (Figure  
400 4).

**Figure 4:**  $N_{2.5-10}$  and  $N_{10}$  as a function of distance from the center of the plume for ETNA13 (a and b) and STRO15 (d, e, g, and h). The plots (g) and (h) are similar to (d) and (e) but with a larger horizontal extent from the center of the plume in STRO15. The considered transects are highlighted by the corresponding colors in the right panel (c for Etna and f for Stromboli).



401 In each transect (highlighted in blue, red, green and purple in Figure 4; c, f), we determined the  
402 center of the plume by the peak of  $\text{SO}_2$  (not shown). The plume widths are of the order of 6-8 km  
403 for the two transects nearest to the volcanoes (respectively at  $\sim 7$  and  $\sim 10$  km from the vent) for  
404 both volcanoes (Figure 4; a, b, d, and e). Further downwind, the STRO15 plume width increases  
405 to about 30 km at  $\sim 80$  km distant from the vent (Figure 4; g, h). For the ETNA13 and STRO15  
406 flights, their corresponding  $N_{2.5-10}$  maxima were not observed at the center of the plume, but at  
407 the edges of the plumes (Figure 4; a, d). Conversely,  $N_{10}$  possesses the maxima exactly at the  
408 center of the plume in the FT (Figure 4; b), whereas in the BL it was also shifted to the plume's  
409 border (Figure 4; e). These results support that the presence of large CS at the center of the  
410 plume is likely to explain the peaks shifting of  $N_{2.5-10}$  (and  $N_{10}$  in the BL), inhibiting the  
411 nucleation process (despite SA continuously produced by oxidation of  $\text{SO}_2$ ) compared to more  
412 favorable conditions at the plume periphery, where the CS is lower. The relationships between  
413 the particle concentrations in the smallest size bin and their gas-phase precursors, as a function of  
414 the distance from the volcanoes' vents, are further investigated in the following section.

### 415 3.3 Derivation of new particle formation parameterization

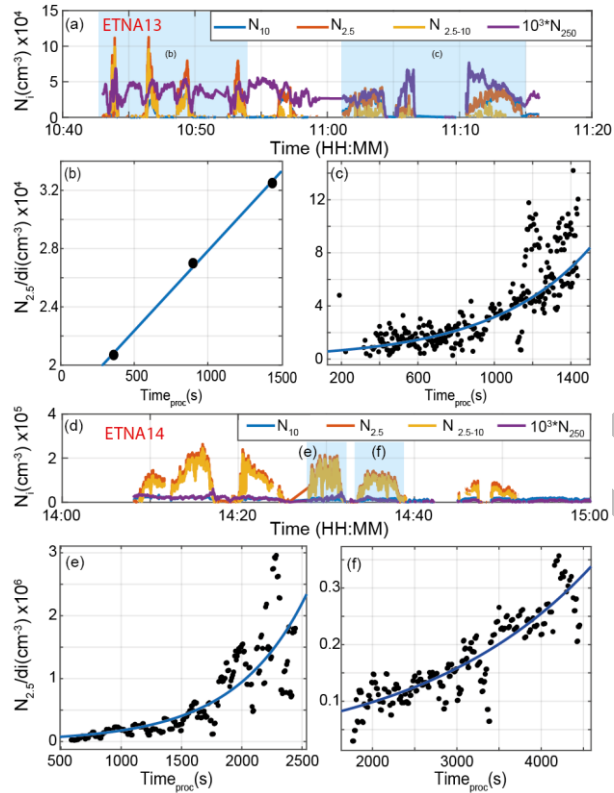
416 The data from the in-situ measurements are used to derive a parameterization that can be  
417 useful to describe the rate of NPF as a function of SA concentration under natural conditions.  
418 One hypothesis in our derivation of the nucleation rate is that losses of newly formed particles  
419 due to coagulation are negligible compared to the strength of the nucleation rate. Thus, we  
420 believe that our calculation is the lower estimate of the nucleation rate within the volcanic  
421 plumes. Nucleation rates were derived when the nucleation mode particle concentrations ( $N_{2.5}$ )  
422 was increasing with processing time ( $t$ ) for several periods and locations, where NPF was  
423 observed to occur (Figure 5, a and d; areas are highlighted by blue). The parameter  $t$  is the time  
424 needed for an air mass originating from the vent to reach the point where it was sampled by the  
425 aircraft. This time is estimated here by integrating the wind speed along the plume with the  
426 distance from the vent as following:

$$t = \frac{x_0}{\bar{V}_x} + \sum_{i=x_0+1}^{i=L} \frac{\Delta x}{V(i)}$$

427  $x_0$  is the distance between the closest point from the flight trajectory inside the volcanic  
428 plume and the vent,  $\bar{V}_x$  is the mean wind speed of all the trajectory points,  $L$  is the farthest point  
429 from the vent of flight trajectory within the plume,  $\Delta x$  is the distance traveled by the aircraft  
430 from the source point (vent) and  $V(i)$  is the corresponding wind speed of each point of the flight  
431 trajectory. Since the nucleation events were found to be more pronounced in the FT than in the  
432 BL, a nucleation rate could only be calculated along the plumes in the FT, and hence the  
433 parameterization is solely based on Etna emissions. We plot the particle concentration increase  
434 as a function of the processing time by taking into account the dilution of the plume with  
435 transport within the plume. It is important to note that the volcanic passive plume at Etna  
436 contains a low concentration of CO (upper limit was 110 ppbV), a typical gas used as a dilution  
437 factor ( $di$ ). Therefore during this study,  $SO_2$  is used as a dilution factor, while its concentration is  
438 strongly enhanced in the plume and has a typical tropospheric average lifetime of 1-2 days  
439 (Beirle et al., 2014), and thus, is partially consumed during the plume evolution. A dilution  
440 factor, defined as the  $SO_2$  concentration normalized by its maximum value for each flight, was  
441 hence applied to the particle concentration to calculate normalized particle number  
442 concentrations. Figure 5 (b, c, e and f) shows the normalized  $N_{2.5}$  concentrations as a function of  
443  $t$  to evaluate the correlation between these two variables. For ETNA13, we divided the flight into  
444 two periods: a) from 10:40 to 10:55 when the aircraft only crossed the plume at different  
445 distances from the vent, and b) from 11:00 to 11:15 when the aircraft was flying within the  
446 center of the plume. For ETNA14, we furthermore chose two periods where the NPF events were  
447 observed to occur at two different altitudes in the FT: c) from 14:28 to 14:32 at  $\sim 2.8$  km and d)  
448 from 14:34 to 14:38  $\sim 3.3$  km. In period (a), we calculated the mean value of each particle peak,  
449 each corresponding to a single processing time (Figure 5; b). The fit of those points against  $t$  was  
450 linear (Figure 5, b), yielding a slope of  $11 \text{ cm}^{-3} \text{ s}^{-1}$ . In period (b), the function between  
451 normalized  $N_{2.5}$  concentrations and the  $t$  was exponential (Figure 5; c). The rate of NPF ( $j_{2.5}$ ) for  
452 each nucleation event is then the derivative of each of the above-mentioned regressions for the  
453 two periods for flight ETNA13. Similarly to the period (b), the regression for the two chosen  
454 periods for flight ETNA14 was found to be exponential as well (Figure 5; e and f).

**Figure 5: Time series of the total number concentration of particles at different cut-off sizes for ETNA13 (a) and ETNA14 (d) with the  $N_{2.5}$  versus processing time with their fitting regressions at different periods (b) 10:40**

to 10:55 UTC, (c) from 11:00 to 11:15 UTC for flight ETNA13, (e) from 14:28 to 14:33 UTC and (f) from 14:34 to 14:38 UTC



455 Table 5 shows all the derived relationships between the normalized  $N_{2.5}$  vs.  $t$  with their  
 456 fitting parameters  $A$  and  $B$  to estimate the nucleation rate  $j_{2.5}$ . The relationship has either a linear  
 457 form as in a period (a) (illustrated in Figure 5; b) or an exponential form as in periods (b, c, and  
 458 d) (illustrated in Figure 5; c, e, and f):  
 459  $j_{2.5} = d(N_{2.5}/di)/dt = A e^{Bt}$  (1)

**Table 5: Summary of the derivative of the correlation between the normalized  $N_{2.5}$  and corresponding processing time shown in Figure 5 (b, c, e, and f) with their fitting parameters for the different periods in the case of ETNA13 and ETNA14 in the free troposphere. The confidence bounds for all regressions were 95%.**

	ETNA13		ETNA14	
<b>Period</b>	(a)	(b)	(c)	(d)
	10:40 to 10:55	11:00 to 11:15	14:28 to 14:32	14:34 to 14:38
<b>Regression of <math>N_{2.5}/di</math> vs <math>t</math></b>	$11 \times t + 17000$	$4505 \times e^{1.95 \times 10^{-3} \times t}$	$32280 \times e^{1.7 \times 10^{-3} \times t}$	$37990 \times e^{4.8 \times 10^{-4} \times t}$
<b><math>j_{2.5} = d(N_{2.5}/di)/dt</math></b>	11	$9 \times e^{1.95 \times 10^{-3} \times t}$	$55 \times e^{1.7 \times 10^{-3} \times t}$	$18 \times e^{4.8 \times 10^{-4} \times t}$
<b><math>R^2</math></b>	0.99	0.8814	0.9123	0.8124
<b>Adjusted <math>R^2</math></b>	0.98	0.881	0.9119	0.8116

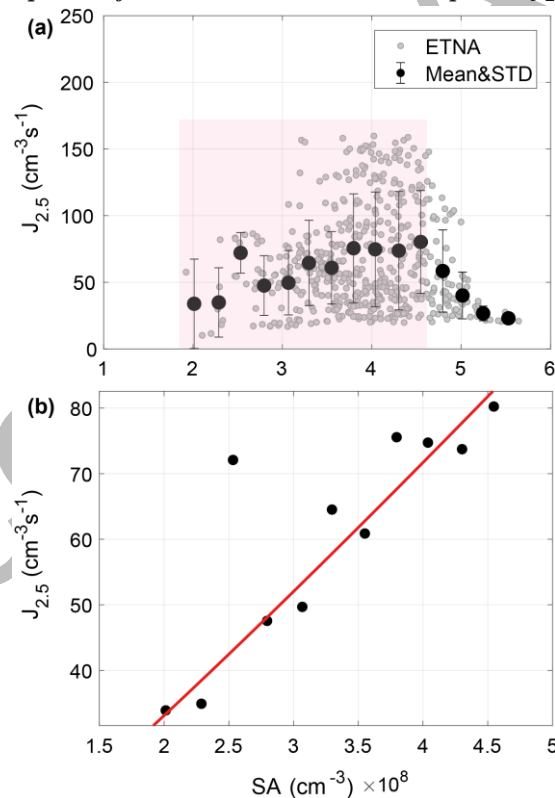
460 Figure 6 shows all estimated  $j_{2.5}$  for all Etna points in the FT versus SA together with their  
 461 averages (black dots) every  $0.25 \times 10^8 \text{ cm}^{-3}$ . We derive the parameterization of NPF rate  $J_{2.5}$  by

462 fitting the averages of all estimated  $J_{2.5}$  to the corresponding SA using the bi-squares method,  
463 with 95% confidence bounds, of the simple power model that has the form:

$$464 \quad J_{2.5} = K[SA]^P \quad (2)$$

465 where pre-factor  $K$  and exponent  $P$  are the fitting parameters of the power function and,  
466 estimated to be  $1.844 \times 10^{-8} \text{ s}^{-1}$  and 1.12 (95% confidence interval 0.76 and 1.47), respectively.  
467 The exponent  $P$ , found in the current study, is closer to 1 (associated with activation-type  
468 nucleation) (Kulmala et al., 2006) rather than kinetic-type nucleation (2) (McMurry &  
469 Friedlander, 1979), in agreement with what has previously been hypothesized (Kuang et al.,  
470 2008; Sihto et al., 2006). According to our derivation and by substituting the values of  $K$ ,  $P$  and  
471 the medians of SA from Table 4 for ETNA13 and ETNA14, the average  $J_{2.5}$  is  $68.6 \pm 39.9$  and  
472  $59.23 \pm 29.8 \text{ cm}^{-3} \text{ s}^{-1}$ , respectively, and equal to  $63.23 \pm 34.8 \text{ cm}^{-3} \text{ s}^{-1}$  for all ETNA points.

**Figure6:** The calculated  $J_{2.5}$  versus SA for the different periods of all ETNA flights in the free troposphere. The black dots and the associated error bars on the panel (a) are the mean and the standard deviation of the  $J_{2.5}$  obtained within  $0.25 \times 10^8 \text{ cm}^{-3}$  SA equal bins. The black dots in panel (b) are the mean  $J_{2.5}$  as a function of SA for the specific SA range defined by the light red shaded area on the panel (a) when SA is smaller than  $4.6 \times 10^8 \text{ cm}^{-3}$ . In the panel (b), the correlation between  $J_{2.5}$  and SA is a power fit (red line), which represents the parameterization of the new particle formation within the volcanic plume  $J_{2.5} = 1.844 \times 10^{-8} [SA]^{1.12}$ .



473 In our derivation, the coagulation process was neglected in comparison to the strength of the  
474 nucleation process, therefore, the  $J_{2.5}$  values derived here are considered as the lower limits of  
475 nucleation. Based on Quantum Chemistry-normalized Classical Nucleation Theory (QC-CNT)  
476 and CLOUD measurements presented in Duplissy et al. (2016), the nucleation of new particles is  
477 minimized when SA was below  $10^8 \text{ cm}^{-3}$  at temperatures above  $10^\circ\text{C}$ . This indicates that the SA  
478 background (up to  $0.85 \times 10^8 \text{ cm}^{-3}$ ), which was subtracted from the data, would not have a  
479 significant impact on our derivation of the NPF rate. Moreover, this parameterization is valid

480 when SA is less than  $4.6 \times 10^8 \text{ cm}^{-3}$  (Figure 6; a). For values of SA larger than  $4.6 \times 10^8$ ,  $J_{2.5}$  has  
481 been observed to significantly decrease with increasing SA (Figure 6; a) due to the large CS  
482 estimated at distances close to the vent (less than 5 km) or in the center of the plume, where  
483 growth is observed to be stronger than NPF. For the SA values greater than  $4.6 \times 10^8 \text{ cm}^{-3}$ , we  
484 believe that the approximation of negligible coagulation is no longer valid. In comparison to  
485 more cleaner environments, our lower limits estimations of  $J_{2.5}$  are one to almost 2 orders of  
486 magnitude higher than what has been previously measured in Hyytiälä (Finland) during the  
487 QUEST2 campaign in 2003 by Sihto et al. (2006) for  $J_3$ . The formation rate  $J_{2.5}$  is a factor of  
488  $\sim 2.5$  to 4 higher than the upper limit of  $J_1$  found for the same campaign (Kuang et al., 2008;  
489 Sihto et al., 2006). These suggest a quicker occurrence of NPF within the harsh environment of  
490 the volcanic passive plume in comparison to what has been found in other cleaner environments  
491 (Sihto et al., 2006). In comparison to the controlled CLOUD3 and CLOUD5 experiments of SA-  
492 water binary particle formation for the same range of SA, our estimation of  $J_{2.5}$  is comparable or  
493 an order of magnitude higher than the  $J$  resulted from the exposure to different beams in the  
494 CLOUD chamber (Figure 9 in Duplissy et al., 2016). This may indicate that condensable vapors  
495 other than SA could be contributing to the NPF events. Indeed, Kirkby et al. (2011) showed that  
496  $\sim 100$  pptV of ammonia may increase nucleation up to a factor of 1000 more than what binary  
497 SA-water nucleation can produce. However, in the absence of chemical characterization, our  
498 observations were not able to confirm the contribution of the other species than sulfuric acid to  
499 the NPF process. Our estimation of  $J_{2.5}$  is found to be more than one order of magnitude higher  
500 than what was estimated, on average, within the aged volcanic plume that reached the puy de  
501 Dôme station, Massif Central (France) ( $4.76 \pm 2.63 \text{ cm}^{-3} \text{ s}^{-1}$ ) in May 2010 from the  
502 Eyjafjallajökull eruption event (Boulon et al., 2011). This is expected since the plume in that  
503 study traveled several thousands of kilometers before reaching the station, whereas our  
504 measurements are occurring directly within the passive plume. This indicates how efficient the  
505 volcanic passive plume can be especially in the free troposphere where new particle formation is  
506 favored. Substituting the average estimated value of SA ( $3.67 \pm 0.78 \times 10^7 \text{ molecules cm}^{-3}$ )  
507 from Boulon et al. (2011) in our parameterization formula (equation 2) would give an NPF rate  
508 of  $5.02 \text{ cm}^{-3} \text{ s}^{-1}$ , which is close to the average nucleation rate actually calculated from the  
509 Eyjafjallajökull plume (Boulon et al., 2011). This indicates that our parameterization would be  
510 able to reproduce the average nucleation rate  $J_2$  estimated for the volcanic plumes even with SA  
511 less than  $10^8 \text{ cm}^{-3}$  at locations far from the eruptive point. Yet, the binary homogeneous  $\text{H}_2\text{SO}_4$ -  
512  $\text{H}_2\text{O}$  nucleation scheme (BHNS) (Kulmala et al., 1998) and activation nucleation (Sihto et al.,  
513 2006) have been used in a previous modeling study that investigated the impact of volcanic  
514 aerosols on climate (Schmidt et al., 2012). The BHNS was found to underestimate the climatic  
515 impact of freshly formed particles in the volcanic degassing plumes (Boulon et al., 2011;  
516 Schmidt et al., 2012). Therefore, our current analysis together with the parameterization can  
517 effectively contribute to better understand and quantify the climatic impacts of aerosol nucleation  
518 and their evolution within volcanic plumes near the volcanic source and in the diluted volcanic  
519 plumes.

#### 520 4 Conclusions

521 This study presents a comprehensive investigation of new particle formation and growth  
522 within volcanic plumes located in the FT and in the BL. This was conducted by performing  
523 airborne in-situ measurements within the plumes of Etna and Stromboli, Italy.

524 We evidenced the occurrence of new particle formation and growth of these newly  
525 formed particles within the different plumes from Etna in the FT and Stromboli in the BL. In the  
526 FT, the NPF events were measured in the volcanic passive plume near the vent with a rapid  
527 growth rate, and continue to occur efficiently along the plume at distances farther than 35 km.  
528 The rapid growth of the newly formed particles was observed close to the vent results in a  
529 relatively high number concentration of large particles ( $N_{250} > 55 \text{ cm}^{-3}$ ) and hence a relatively  
530 significant CS (up to  $10^{-2} \text{ s}^{-1}$  in absolute value). However, the concentration of these large  
531 particles is diluted with distance, and therefore the threshold ratio between the condensable gases  
532 and the condensational sink is overcome by the presence of sufficient SA from  $\text{SO}_2$  oxidation to  
533 allow for further nucleation events. In the BL, the NPF events were also observed close to the  
534 vent of the volcano and with smaller concentrations of ultrafine particles than in the FT. The  $\text{SO}_2$   
535 fluxes at Stromboli were reported to be weak (0.15-0.6 kt/day, (Burton et al., 2008)), but they  
536 remain comparable with those emitted at Etna during passive degassing (0.6-2 kt/day, (Aiuppa et  
537 al., 2008; Roberts et al., 2018)). This has been supported by our observations, where we found  
538 that  $\text{SO}_2$  and SA concentrations were relatively comparable and the differences in their values in  
539 different volcanic plumes of Etna (being passive) and Stromboli are small. Thus, these small  
540 differences in  $\text{SO}_2$  and SA concentrations between Etna and Stromboli do not explain solely the  
541 NPF being more dominant in Etna (in the FT) than in Stromboli (in the BL). Therefore, the  
542 occurrence of the NPF events in the different volcanic plumes seems to be largely influenced by  
543 the presence of large particles leading to large CS at the very proximity to the vent. Thus, the  
544 weaker NPF events in the BL is a result of a larger aerosol surface along the plume, where CS  
545 was up to 2 orders of magnitude higher than in the FT, and with temperatures reaching 23 and 30  
546 °C in both BL flights, which is up to 20°C higher than in the FT. This detailed analysis of the  
547 growth of freshly nucleated particles to the CCN sizes (Figure S4 and S5) is beneficial for further  
548 modeling studies to investigate the contribution of NPF to the CCN and their impact on climate.

549 To the authors' knowledge, this is the first dedicated study that addresses the relationship  
550 between the newly formed nanoparticles and their gas-phase precursors in the vicinity of  
551 different volcanic plumes over Etna and Stromboli. The in-situ airborne measurements  
552 performed as part of this study within the ETNA passive plume were used to derive NPF rate  
553 parameterizations  $J_{2.5}$  that can eventually be incorporated into models. The NPF rate was an  
554 exponential function of the processing time in most of the observed individual nucleation events  
555 along the flight trajectories and implicitly includes the information about the plume's dilution.  
556 The NPF rate parameterization was a power law function of SA, with an exponent value of 1.12,  
557 which is accepted within the range of what has previously been reported (Kuang et al., 2008;  
558 Sihto et al., 2006). The latter exponent value implies that the nucleation within the studied  
559 plumes is a natural process that is a mixture of both activation (Kulmala et al., 2006) and kinetic  
560 (McMurry & Friedlander, 1979) nucleation modes, but more close to the activation nucleation  
561 mode. We believe that our calculation is the lower estimate of the nucleation rate within the  
562 volcanic plume since the losses due to coagulation are neglected compared to the strength of the  
563 nucleation rate. This new parameterization has a simple formula and is able to reproduce the  
564 same average nucleation rate for the volcanic plumes observed in locations thousands of  
565 kilometers distant from the erupted event (Boulon et al., 2011). Therefore, this parametrization  
566 of particle formation rate, based on actual measurements, is a more representative of the  
567 nucleation process occurred under largely uncharacterized volcanic degassing plumes conditions.  
568 The new parametrization should further be tested in mesoscale models coupled with chemistry  
569 transport scheme and compared with pre-existing parametrizations for new particle formation

570 within volcanic plumes. It should be noted that although SA is the key factor for the NPF events  
571 within the different volcanic plumes, we cannot exclude that condensable vapors other than SA,  
572 e.g. halogens and organic vapors, could be participating to the nucleation and growth processes  
573 in the FT and BL, and the latter should be investigated by deeper chemical characterization in  
574 future studies. Finally, this study contributes to better understand and quantify the natural  
575 process of the gas to particle conversion within volcanic plumes, and how this process with the  
576 resulted aerosol concentrations evolves temporally and spatially in the atmosphere aiming to  
577 reduce the uncertainty of the aerosol's impact on climate.

## 578 Acknowledgments

579 The authors would like to thank the three anonymous reviewers for their constructive  
580 comments and suggestions, which contributed significantly to the improvement of the article.

581 The data of these measurements are possessed by the STRAP program and available on  
582 STRAP website <http://osur.univ-reunion.fr/recherche/strap/database/>. The lead author and this  
583 work are funded by the ClerVolc project - Programme 1 "Detection and characterization of  
584 volcanic plumes and ash clouds" funded by the French government 'Laboratory of Excellence'  
585 initiative, ClerVolc contribution number 311. The authors would like to extend a special thanks  
586 to the pilots and flight crew from SAFIRE for all their enthusiasm and support during the  
587 measurement campaign aboard the ATR-42 aircraft. We would also like to thank Dr. Douglas R.  
588 Worsnop, Vice President/Director in Aerodyne Incorporation, for the information to develop the  
589 ambient ionization inlet to be used with the APi-ToF instrument onboard.

## 590 References

- 591 Aiuppa, A., Federico, C., Giudice, G., Gurrieri, S., Liuzzo, M., Shinohara, H., et al. (2006). Rates of carbon dioxide  
592 plume degassing from Mount Etna volcano. *Journal of Geophysical Research*, *111*(B9), B09207.  
593 <https://doi.org/10.1029/2006JB004307>
- 594 Aiuppa, A., Giudice, G., Gurrieri, S., Liuzzo, M., Burton, M., Caltabiano, T., et al. (2008). Total volatile flux from  
595 Mount Etna. *Journal of Geophysical Research*, *35*, 12809–12819. <https://doi.org/10.1029/2008GL035871>
- 596 Albrecht, B. A. (1989). Aerosols, Cloud Microphysics, and Fractional Cloudiness. *Science*, *245*(4923), 1227–1230.  
597 <https://doi.org/10.1126/science.245.4923.1227>
- 598 Allard, P., Carbonnelle, J., Dajčević, D., Bronec, J. L., Morel, P., Robe, M. C., et al. (1991). Eruptive and diffuse  
599 emissions of CO<sub>2</sub> from Mount Etna. *Nature*, *351*(6325), 387–391. <https://doi.org/10.1038/351387a0>
- 600 Allard, P., Aiuppa, A., Loyer, H., Carrot, F., Gaudry, A., Pinte, G., et al. (2000). Acid gas and metal emission rates  
601 during long-lived basalt degassing at Stromboli volcano. *Geophysical Research Letters*, *27*(8), 1207–1210.  
602 <https://doi.org/10.1029/1999GL008413>
- 603 Andres, R. J., & Kasgnoc, a. D. (1998). A time-averaged inventory of subaerial volcanic sulfur emissions. *J.*  
604 *Geophys. Res.*, *103*(D19), 25251. <https://doi.org/10.1029/98JD02091>
- 605 Beirle, S., Hörmann, C., Vries, M. P. De, Dörner, S., Kern, C., & Wagner, T. (2014). Estimating the volcanic  
606 emission rate and atmospheric lifetime of SO<sub>2</sub> from space : a case study for Kilauea volcano , Hawai ' i,  
607 8309–8322. <https://doi.org/10.5194/acp-14-8309-2014>
- 608 Blackburn, E. A., Wilson, L., & Sparks, R. J. (1976). Mechanisms and dynamics of strombolian activity. *Journal of*  
609 *the Geological Society*, *132*, 429–440.
- 610 Bobrowski, N., Glasow, R. Von, Aiuppa, A., Inguaggiato, S., Louban, I., & Ibrahim, O. W. (2007). Reactive  
611 halogen chemistry in volcanic plumes, *112*(November 2006), 1–17. <https://doi.org/10.1029/2006JD007206>
- 612 Boulon, J., Sellegri, K., Hervé, M., & Laj, P. (2011). Observations of nucleation of new particles in a volcanic  
613 plume. *Proceedings of the National Academy of Sciences of the United States of America*, *108*(30), 12223–6.  
614 <https://doi.org/10.1073/pnas.1104923108>
- 615 Burton, M. R., Caltabiano, T., Murè, F., Salerno, G., & Randazzo, D. (2008). SO<sub>2</sub> flux from Stromboli during the  
616 2007 eruption: Results from the FLAME network and traverse measurements. *Journal of Volcanology and*  
617 *Geothermal Research*, *182*, 214–220. <https://doi.org/10.1016/j.jvolgeores.2008.11.025>
- 618 Caltabiano, T., Romano, R., & Budetta, G. (1994). SO<sub>2</sub> flux measurements at Mount Etna ( Sicily ). *Journal of*

- 619 *Geophysical Research*, 99(94), 12809–12819.
- 620 Calvari, S., Salerno, G. G., Spampinato, L., Gouhier, M., Spina, A. La, Pecora, E., et al. (2011). An unloading foam  
621 model to constrain Etna's 11–13 January 2011 lava fountaining episode. *Journal of Geophysical Research*,  
622 116(January), 1–18. <https://doi.org/10.1029/2011JB008407>
- 623 Carn, S. A., Krotkov, N. A., Yang, K., & Krueger, A. J. (2013). Measuring global volcanic degassing with the  
624 Ozone Monitoring Instrument (OMI). *Geological Society, London, Special Publications*, 380(1), 229–257.  
625 <https://doi.org/10.1144/SP380.12>
- 626 Carn, S. A., Clarisse, L., & Prata, A. J. (2016). Multi-decadal satellite measurements of global volcanic degassing.  
627 *Journal of Volcanology and Geothermal Research*, 311, 99–134.  
628 <https://doi.org/10.1016/J.JVOLGEORES.2016.01.002>
- 629 Carslaw, K. S., Lee, L. A., Reddington, C. L., Pringle, K. J., Rap, A., Forster, P. M., et al. (2013). Large contribution  
630 of natural aerosols to uncertainty in indirect forcing. *Nature*, 503(7474), 67–71.  
631 <https://doi.org/10.1038/nature12674>
- 632 Delmelle, P. (2003). Environmental impacts of tropospheric volcanic gas plumes. *Geological Society, London,*  
633 *Special Publications*, 213(1), 381–399. <https://doi.org/10.1144/GSL.SP.2003.213.01.23>
- 634 Draxler, R. R. (2003). Evaluation of an Ensemble Dispersion Calculation. *Journal of Applied Meteorology*, 42(2),  
635 308–317. [https://doi.org/https://doi.org/10.1175/1520-0450\(2003\)042<0308:EOAEDC>2.0.CO;2](https://doi.org/https://doi.org/10.1175/1520-0450(2003)042<0308:EOAEDC>2.0.CO;2)
- 636 Duplissy, J., Merikanto, J., Franchin, A., Tsagkogeorgas, G., Kangasluoma, J., Wimmer, D., et al. (2016). Effect of  
637 ions on sulfuric acid-water binary particle formation: 2. Experimental data and comparison with QC-  
638 normalized classical nucleation theory. *Journal of Geophysical Research: Atmospheres*, 121(4), 1752–1775.  
639 <https://doi.org/10.1002/2015JD023539>
- 640 Galle, B., Johansson, M., Rivera, C., Zhang, Y., Kihlman, M., Kern, C., et al. (2010). Network for Observation of  
641 Volcanic and Atmospheric Change (NOVAC)—A global network for volcanic gas monitoring: Network  
642 layout and instrument description. *Journal of Geophysical Research*, 115(D5), D05304.  
643 <https://doi.org/10.1029/2009JD011823>
- 644 Gassó, S. (2008). Satellite observations of the impact of weak volcanic activity on marine clouds. *Journal of*  
645 *Geophysical Research*, 113(D14), D14S19. <https://doi.org/10.1029/2007JD009106>
- 646 Gordon, H., Sengupta, K., Rap, A., Duplissy, J., Frege, C., Williamson, C., et al. (2016). Reduced anthropogenic  
647 aerosol radiative forcing caused by biogenic new particle formation. *PNAS*, 113(43), 12053–12058.  
648 <https://doi.org/10.1073/pnas.1602360113>
- 649 Gordon, H., Kirkby, J., Baltensperger, U., Bianchi, F., Breitenlechner, M., Curtius, J., et al. (2017). Causes and  
650 importance of new particle formation in the present-day and preindustrial atmospheres. *Journal of*  
651 *Geophysical Research: Atmospheres*, 122(16), 8739–8760. <https://doi.org/10.1002/2017JD026844>
- 652 GRIMM. (2008). Specification for Model 1.129 Sky-Optical Particle Counter (full version). *Users' Manual*, 1–44.  
653 Retrieved from [www.grimm-aerosol.com](http://www.grimm-aerosol.com)
- 654 Haywood, J., & Boucher, O. (2000). Estimates of the direct and indirect radiative forcing due to tropospheric  
655 aerosols: A review. *Reviews of Geophysics*, 38(4), 513–543. <https://doi.org/10.1029/1999RG000078>
- 656 Hobbs, P. V., Tuell, J. P., Hegg, D. A., Radke, L. F., & Eltgroth, M. W. (1982). Particles and gases in the emissions  
657 from the 1980–1981 volcanic eruptions of Mt. St. Helens. *Journal of Geophysical Research*, 87(C13), 11062.  
658 <https://doi.org/10.1029/JC087iC13p11062>
- 659 Hoyle, C. R., Pinti, V., Welti, A., Zobrist, B., Marcolli, C., Luo, B., et al. (2011). Ice nucleation properties of  
660 volcanic ash from Eyjafjallajökull. *Atmos. Chem. Phys. Atmospheric Chemistry and Physics*, 11, 9911–9926.  
661 <https://doi.org/10.5194/acp-11-9911-2011>
- 662 Ilyinskaya, E., Martin, R. S., & Oppenheimer, C. (2012). Aerosol formation in basaltic lava fountaining:  
663 Eyjafjallajökull volcano, Iceland. *Journal of Geophysical Research: Atmospheres*, 117(D20).  
664 <https://doi.org/10.1029/2011JD016811>
- 665 Ilyinskaya, E., Schmidt, A., Mather, T. A., Pope, F. D., Witham, C., Baxter, P., et al. (2017). Understanding the  
666 environmental impacts of large fissure eruptions: Aerosol and gas emissions from the 2014–2015 Holuhraun  
667 eruption (Iceland). *Earth and Planetary Science Letters*, 472, 309–322.  
668 <https://doi.org/10.1016/j.epsl.2017.05.025>
- 669 Junninen, H., Ehn, M., Petäjä, T., Luosujärvi, L., Kotiaho, T., Kostianen, R., et al. (2010). A high-resolution mass  
670 spectrometer to measure atmospheric ion composition. *Atmospheric Measurement Techniques*, 3(4), 1039–  
671 1053. <https://doi.org/10.5194/amt-3-1039-2010>
- 672 Kantzas, E. P., & McGonigle, A. J. S. (2008). Ground Based Ultraviolet Remote Sensing of Volcanic Gas Plumes.  
673 *Sensors (Basel, Switzerland)*, 8(3), 1559–1574. <https://doi.org/10.3390/s8031559>
- 674 Kerminen, V.-M., Paramonov, M., Anttila, T., Riipinen, I., Fountoukis, C., Korhonen, H., et al. (2012). Cloud

- 675 condensation nuclei production associated with atmospheric nucleation: a synthesis based on existing  
676 literature and new results. *Atmospheric Chemistry and Physics*, 12(24), 12037–12059.  
677 <https://doi.org/10.5194/acp-12-12037-2012>
- 678 Kirkby, J., Curtius, J., Almeida, J., Dunne, E., Duplissy, J., Ehrhart, S., et al. (2011). Role of sulphuric acid,  
679 ammonia and galactic cosmic rays in atmospheric aerosol nucleation. *Nature*, 476(7361), 429–433.  
680 <https://doi.org/10.1038/nature10343>
- 681 Kroll, J. H., Cross, E. S., Hunter, J. F., Pai, S., Wallace, L. M. M., Croteau, P. L., et al. (2015). Atmospheric  
682 evolution of sulfur emissions from Kilauea: Real-time measurements of oxidation, dilution, and neutralization  
683 within a volcanic plume. *Environmental Science and Technology*, 49(7), 4129–4137.  
684 <https://doi.org/10.1021/es506119x>
- 685 Kuang, C., McMurry, P. H., McCormick, A. V., & Eisele, F. L. (2008). Dependence of nucleation rates on sulfuric  
686 acid vapor concentration in diverse atmospheric locations. *Journal of Geophysical Research Atmospheres*,  
687 113(10), 1–9. <https://doi.org/10.1029/2007JD009253>
- 688 Kulmala, M., & Kerminen, V.-M. (2008). On the formation and growth of atmospheric nanoparticles. *Atmospheric  
689 Research*, 90(2–4), 132–150. <https://doi.org/10.1016/J.ATMOSRES.2008.01.005>
- 690 Kulmala, M., & Laaksonen, A. (1990). Binary nucleation of water–sulfuric acid system: Comparison of classical  
691 theories with different H<sub>2</sub>SO<sub>4</sub> saturation vapor pressures. *The Journal of Chemical Physics*, 93(1), 696–701.  
692 <https://doi.org/10.1063/1.459519>
- 693 Kulmala, M., Laaksonen, A., & Pirjola, L. (1998). Parameterizations for sulfuric acid/water nucleation rates.  
694 *Journal of Geophysical Research Atmospheres*, 103(D7), 8301–8307. <https://doi.org/10.1029/97JD03718>
- 695 Kulmala, M., Dal Maso, M., Mäkelä, J. M., Pirjola, L., Väkevä, M., Aalto, P., et al. (2001). On the formation,  
696 growth and composition of nucleation mode particles. *Tellus, Series B: Chemical and Physical Meteorology*,  
697 53(4), 479–490. <https://doi.org/10.1034/j.1600-0889.2001.d01-33.x>
- 698 Kulmala, M., Vehkamäki, H., Petäjä, T., Dal Maso, M., Lauri, A., Kerminen, V. M., et al. (2004). Formation and  
699 growth rates of ultrafine atmospheric particles: A review of observations. *Journal of Aerosol Science*, 35(2),  
700 143–176. <https://doi.org/10.1016/j.jaerosci.2003.10.003>
- 701 Kulmala, M., Lehtinen, K. E. J., & Laaksonen, A. (2006). Cluster activation theory as an explanation of the linear  
702 dependence between formation rate of 3 nm particles and sulphuric acid concentration. *Atmos. Chem. Phys.*  
703 *Atmospheric Chemistry and Physics*, 6, 787–793. Retrieved from [www.atmos-chem-phys.net/6/787/2006/](http://www.atmos-chem-phys.net/6/787/2006/)  
704 Kulmala, M., Petäjä, T., Ehn, M., Thornton, J., Sipilä, M., Worsnop, D. R., & Kerminen, V.-M. (2014). Chemistry  
705 of Atmospheric Nucleation: On the Recent Advances on Precursor Characterization and Atmospheric Cluster  
706 Composition in Connection with Atmospheric New Particle Formation. *Annual Review of Physical Chemistry*,  
707 65(1), 21–37. <https://doi.org/10.1146/annurev-physchem-040412-110014>
- 708 Kupc, A., Bischof, O., Tritscher, T., Beeston, M., Krinke, T., & Wagner, P. E. (2013). Laboratory Characterization  
709 of a New Nano-Water- Based CPC 3788 and Performance Comparison to an Ultrafine Butanol-Based CPC  
710 3776 Laboratory Characterization of a New Nano-Water-Based CPC 3788 and Performance Comparison to an  
711 Ultrafine Butanol-Based CPC 3776. *Aerosol Science and Technology*, 47(47).  
712 <https://doi.org/10.1080/02786826.2012.738317>
- 713 Makkonen, R., Asmi, A., Kerminen, V.-M., Boy, M., Arneth, A., Hari, P., & Kulmala, M. (2012). Air pollution  
714 control and decreasing new particle formation lead to strong climate warming. *Atmospheric Chemistry and  
715 Physics*, 12(3), 1515–1524. <https://doi.org/10.5194/acp-12-1515-2012>
- 716 Mather, T. A. (2015). Volcanoes and the environment: Lessons for understanding Earth’s past and future from  
717 studies of present-day volcanic emissions. *Journal of Volcanology and Geothermal Research*, 304, 160–179.  
718 <https://doi.org/10.1016/j.jvolgeores.2015.08.016>
- 719 Mather, T. A., & Pyle, D. M. (2015). Volcanic emissions: short-term perturbations, long-term consequences and  
720 global environmental change. In A. Schmidt, K. E. Fristad, & L. T. Elkins-Tanton (Eds.), *Volcanism and  
721 Global Environmental Change*. Cambridge: Cambridge University Press.  
722 <https://doi.org/10.1017/CBO9781107415683>
- 723 Mather, T. A., Pyle, D. M., & Oppenheimer, C. (2003). Tropospheric volcanic aerosol (pp. 189–212). American  
724 Geophysical Union. <https://doi.org/10.1029/139GM12>
- 725 Mather, T. A., Oppenheimer, C., Allen, A. G., & McGonigle, A. J. S. (2004). Aerosol chemistry of emissions from  
726 three contrasting volcanoes in Italy. *Atmospheric Environment*, 38(33), 5637–5649.  
727 <https://doi.org/10.1016/J.ATMOSENV.2004.06.017>
- 728 Mauldin, R. L., Cantrell, C. A., Zondlo, M., Kosciuch, E., Eisele, F. L., Chen, G., et al. (2003). Highlights of OH,  
729 H<sub>2</sub>SO<sub>4</sub>, and methane sulfonic acid measurements made aboard the NASA P-3B during Transport and  
730 Chemical Evolution over the Pacific, 108, 1–13. <https://doi.org/10.1029/2003JD003410>

- 731 McCormick, K. B., Edmonds, M., & Biggs, J. (2016). Observing eruptions of gas-rich compressible magmas from  
732 space. *Nature Communications*, 7, 13744. <https://doi.org/10.1038/ncomms13744>
- 733 McGonigle, A. J. S., & Oppenheimer, C. (2003). Optical sensing of volcanic gas and aerosol emissions. *Geological*  
734 *Society Special Publication*, 213(January), 149–168. <https://doi.org/10.1144/GSL.SP.2003.213.01.09>
- 735 McGonigle, A. J. S., Pering, T. D., Wilkes, T. C., Tamburello, G., D'Aleo, R., Bitetto, M., et al. (2017). Ultraviolet  
736 Imaging of Volcanic Plumes: A New Paradigm in Volcanology. *Geosciences*, 7(3), 68.  
737 <https://doi.org/10.3390/geosciences7030068>
- 738 McMurry, P. H., & Friedlander, S. K. (1979). New particle formation in the presence of an aerosol. *Atmospheric*  
739 *Environment (1967)*, 13(12), 1635–1651. [https://doi.org/10.1016/0004-6981\(79\)90322-6](https://doi.org/10.1016/0004-6981(79)90322-6)
- 740 Merikanto, J., Spracklen, D. V., Mann, G. W., Pickering, S. J., & Carslaw, K. S. (2009). Impact of nucleation on  
741 global CCN. *Atmos. Chem. Phys. Atmospheric Chemistry and Physics*, 9, 8601–8616. Retrieved from  
742 [www.atmos-chem-phys.net/9/8601/2009/](http://www.atmos-chem-phys.net/9/8601/2009/)
- 743 Model T100U Trace Level Sulfur Dioxide Analyzer. (2011). *Users' Manual*, (August).
- 744 National Institute of Geophysics and Volcanology. (2016). *Bollettino settimanale sul monitoraggio vulcanico,*  
745 *geochimico e sismico del vulcano Etna, Rep. N° 25/2016*. Retrieved from  
746 <http://www.ct.ingv.it/en/rapporti/multidisciplinari.html?view=docman&start=195>
- 747 Naughton, J. J., Lewis, V., Thomas, D., & Finlayson, J. B. (1975). Fume compositions found at various stages of  
748 activity at Kilauea Volcano, Hawaii. *Journal of Geophysical Research*, 80(21), 2963–2966.  
749 <https://doi.org/10.1029/JC080i021p02963>
- 750 Oppenheimer, C., Pyle, D. M. (David M. ., & Barclay, J. (Jenni). (2003). *Volcanic degassing*. Geological Society.  
751 Retrieved from [https://books.google.fr/books?hl=en&lr=&id=zsPoH-](https://books.google.fr/books?hl=en&lr=&id=zsPoH-aCJqWC&oi=fnd&pg=PA1&dq=does+degassing+volcanic+plume+contain+volcanic+ash&ots=z92tWRuquM&sig=iOxAN0eZXyUqa_MsyuUjcdRQKxM#v=onepage&q=does+degassing+volcanic+plume+contain+volcanic+ash&f=false)  
752 [aCJqWC&oi=fnd&pg=PA1&dq=does+degassing+volcanic+plume+contain+volcanic+ash&ots=z92tWRuquM](https://books.google.fr/books?hl=en&lr=&id=zsPoH-aCJqWC&oi=fnd&pg=PA1&dq=does+degassing+volcanic+plume+contain+volcanic+ash&ots=z92tWRuquM&sig=iOxAN0eZXyUqa_MsyuUjcdRQKxM#v=onepage&q=does+degassing+volcanic+plume+contain+volcanic+ash&f=false)  
753 [&sig=iOxAN0eZXyUqa\\_MsyuUjcdRQKxM#v=onepage&q=does degassing volcanic plume contain volcanic](https://books.google.fr/books?hl=en&lr=&id=zsPoH-aCJqWC&oi=fnd&pg=PA1&dq=does+degassing+volcanic+plume+contain+volcanic+ash&ots=z92tWRuquM&sig=iOxAN0eZXyUqa_MsyuUjcdRQKxM#v=onepage&q=does+degassing+volcanic+plume+contain+volcanic+ash&f=false)  
754 [ash&f=false](https://books.google.fr/books?hl=en&lr=&id=zsPoH-aCJqWC&oi=fnd&pg=PA1&dq=does+degassing+volcanic+plume+contain+volcanic+ash&ots=z92tWRuquM&sig=iOxAN0eZXyUqa_MsyuUjcdRQKxM#v=onepage&q=does+degassing+volcanic+plume+contain+volcanic+ash&f=false)
- 755 Oppenheimer, C., Kyle, P., Eisele, F., Crawford, J., Huey, G., Tanner, D., et al. (2010). Atmospheric chemistry of an  
756 Antarctic volcanic plume. *Journal of Geophysical Research Atmospheres*, 115(4), 1–15.  
757 <https://doi.org/10.1029/2009JD011910>
- 758 Oppenheimer, C., Scaillet, B., & Martin, R. S. (2011). Sulfur Degassing From Volcanoes: Source Conditions,  
759 Surveillance, Plume Chemistry and Earth System Impacts. *Reviews in Mineralogy and Geochemistry*, 73(1),  
760 363–421. <https://doi.org/10.2138/rmg.2011.73.13>
- 761 Petäjä, T., Sipilä, M., Paasonen, P., Nieminen, T., Kurtén, T., Ortega, I. K., et al. (2011). Experimental Observation  
762 of Strongly Bound Dimers of Sulfuric Acid: Application to Nucleation in the Atmosphere. *Physical Review*  
763 *Letters*, 106(22), 228302. <https://doi.org/10.1103/PhysRevLett.106.228302>
- 764 Petäjä, T., Laakso, L., Grönholm, T., Launainen, S., Evele-Peltoniemi, I., Virkkula, A., et al. (2012). In-situ  
765 observations of Eyjafjallajökull ash particles by hot-air balloon. *Atmospheric Environment*, 48, 104–112.  
766 <https://doi.org/10.1016/J.ATMOENV.2011.08.046>
- 767 Pirjola, L., Markku, K., Martin, W., Albrecht, B., Frank, S., & Eckhard, O. (1999). Formation of sulphuric acid  
768 aerosols and cloud condensation nuclei: An expression for significant nucleation and model comparison.  
769 *Journal of Aerosol Science*, 30(8), 1079–1094. [https://doi.org/10.1016/S0021-8502\(98\)00776-9](https://doi.org/10.1016/S0021-8502(98)00776-9)
- 770 Pyle, D. M., & Mather, T. A. (2003). The importance of volcanic emissions for the global atmospheric mercury  
771 cycle. *Atmospheric Environment*, 37(36), 5115–5124. <https://doi.org/10.1016/J.ATMOENV.2003.07.011>
- 772 Radke, L. F. (1982). Sulphur and Sulphate from Mt Erebus. *Nature*, 299, 710–712.
- 773 Roberts, T. J., Vignelles, D., Liuzzo, M., Giudice, G., Aiuppa, A., Coltelli, M., et al. (2018). The primary volcanic  
774 aerosol emission from Mt Etna: Size-resolved particles with SO<sub>2</sub> and role in plume reactive halogen  
775 chemistry. *Geochimica et Cosmochimica Acta*, 222, 74–93. <https://doi.org/10.1016/J.GCA.2017.09.040>
- 776 Robock, A. (2000). Volcanic eruptions and climate. *Reviews of Geophysics*, 38(2), 191–219.  
777 <https://doi.org/10.1029/1998RG000054>
- 778 Rondo, L., Ehrhart, S., Kürten, A., Adamov, A., Bianchi, F., Breitenlechner, M., et al. (2016). Effect of  
779 dimethylamine on the gas phase sulfuric acid concentration measured by Chemical Ionization Mass  
780 Spectrometry. *Journal of Geophysical Research: Atmospheres*, 121(6), 3036–3049.  
781 <https://doi.org/10.1002/2015JD023868>
- 782 Rose, W. I., & Durant, A. J. (2009). Fine ash content of explosive eruptions. *Journal of Volcanology and*  
783 *Geothermal Research*, 186(1–2), 32–39. <https://doi.org/10.1016/j.jvolgeores.2009.01.010>
- 784 Rose, W. I., Millard, G. A., Mather, T. A., Hunton, D. E., Anderson, B., Oppenheimer, C., et al. (2006).  
785 Atmospheric chemistry of a 33–34 hour old volcanic cloud from Hekla Volcano (Iceland): Insights from direct  
786 sampling and the application of chemical box modeling. *Journal of Geophysical Research Atmospheres*,

- 787 111(20), 1–17. <https://doi.org/10.1029/2005JD006872>
- 788 Schmidt, A., Ostro, B., Carslaw, K. S., Wilson, M., Thordarson, T., Mann, G. W., & Simmons, A. J. (2011). Excess  
789 mortality in Europe following a future Laki-style Icelandic eruption. *Proceedings of the National Academy of*  
790 *Sciences of the United States of America*, 108(38), 15710–5. <https://doi.org/10.1073/pnas.1108569108>
- 791 Schmidt, A., Carslaw, K. S., Mann, G. W., Rap, A., Pringle, K. J., Spracklen, D. V., et al. (2012). Importance of  
792 tropospheric volcanic aerosol for indirect radiative forcing of climate. *Atmospheric Chemistry and Physics*,  
793 12(16), 7321–7339. <https://doi.org/10.5194/acp-12-7321-2012>
- 794 Schmidt, A., Leadbetter, S., Theys, N., Carboni, E., Witham, C. S., Stevenson, J. A., et al. (2015). Satellite  
795 detection, long-range transport, and air quality impacts of volcanic sulfur dioxide from the 2014–2015 flood  
796 lava eruption at Bárðarbunga (Iceland). *Journal of Geophysical Research: Atmospheres*, 120(18), 9739–9757.  
797 <https://doi.org/10.1002/2015JD023638>
- 798 Seidel, D. J., Zhang, Y., Beljaars, A., Golaz, J.-C., Jacobson, A. R., Medeiros, B., et al. (2012). Climatology of the  
799 planetary boundary layer over the continental United States and Europe. *J. Geophys. Res.*, 117, 17106.  
800 <https://doi.org/10.1029/2012JD018143>
- 801 Sihto, S.-L., Kulmala, M., Kerminen, V.-M., Dal Maso, M., Petäjä, T., Riipinen, I., et al. (2006). Atmospheric  
802 sulphuric acid and aerosol formation: implications from atmospheric measurements for nucleation and early  
803 growth mechanisms. *Atmospheric Chemistry and Physics*, 6(12), 4079–4091. [https://doi.org/10.5194/acp-6-](https://doi.org/10.5194/acp-6-4079-2006)  
804 4079-2006
- 805 Simpson, D., Winiwarter, W., Börjesson, G., Cinderby, S., Ferreira, A., Guenther, A., et al. (1999). Inventorying  
806 emissions from nature in Europe. *Journal of Geophysical Research: Atmospheres*, 104(D7), 8113–8152.  
807 <https://doi.org/10.1029/98JD02747>
- 808 Sipilä, M., Berndt, T., Petäjä, T., Brus, D., Vanhanen, J., Stratmann, F., et al. (2010). The role of sulfuric acid in  
809 atmospheric nucleation. *Science (New York, N.Y.)*, 327(5970), 1243–6.  
810 <https://doi.org/10.1126/science.1180315>
- 811 Smith, S. J., Van Aardenne, J., Klimont, Z., Andres, R. J., Volke, A., & Delgado Arias, S. (2011). Anthropogenic  
812 sulfur dioxide emissions: 1850–2005. *Atmospheric Chemistry and Physics*, 11(3), 1101–1116.  
813 <https://doi.org/10.5194/acp-11-1101-2011>
- 814 Stein, F. A., Draxler, R. R., Rolph, G. D., Stunder, J., Cohen, M. D., & Ngan, F. (2016). NOAA'S HYSPLIT  
815 Atmospheric transport and dispersion modeling system. *Journal of Applied Meteorology and Climatology*,  
816 96(12), 2059–2077. <https://doi.org/10.1175/BAMS-D-14-00110.1>
- 817 Tomasi, C., & Lupi, A. (2016). Primary and Secondary Sources of Atmospheric Aerosol. *Atmospheric Aerosols*, 1–  
818 86. <https://doi.org/10.1002/9783527336449.ch1>
- 819 Tulet, P., Muro, A. Di, Colomb, A., Denjean, C., DufLOT, V., Arellano, S., et al. (2017). First results of the Piton de  
820 la Fournaise STRAP 2015 experiment: multidisciplinary tracking of a volcanic gas and aerosol plume. *Atmos.*  
821 *Chem. Phys.*, 17, 5355–5378. <https://doi.org/10.5194/acp-17-5355-2017>
- 822 Vignelles, D., Roberts, T. J., Carboni, E., Ilyinskaya, E., Pfeffer, M., Dagsson Waldhauserova, P., et al. (2016).  
823 Balloon-borne measurement of the aerosol size distribution from an Icelandic flood basalt eruption. *Earth and*  
824 *Planetary Science Letters*, 453, 252–259. <https://doi.org/10.1016/j.epsl.2016.08.027>
- 825 Volcanology, N. I. of G. and. (2016). *Bollettino settimanale sul monitoraggio vulcanico, geochimico, delle*  
826 *deformazioni del suolo e sismico del vulcano Stromboli, Rep. N° 25/2016*. Retrieved from  
827 <http://www.ct.ingv.it/en/rapporti/multidisciplinari.html?view=docman&start=195>
- 828 Watson, I. M., & Oppenheimer, C. (2000). Particle size distributions of Mount Etna's aerosol plume constrained by  
829 Sun photometry. *Journal of Geophysical Research Atmospheres*, 105(D8), 9823–9829.  
830 <https://doi.org/10.1029/2000JD900042>
- 831 Weber, K., Eliasson, J., Vogel, A., Fischer, C., Pohl, T., Van Haren, G., et al. (2012). Airborne in-situ investigations  
832 of the Eyjafjallajökull volcanic ash plume on Iceland and over north-western Germany with light aircrafts and  
833 optical particle counters. <https://doi.org/10.1016/j.atmosenv.2011.10.030>
- 834 Weber, R. J., Marti, J. J., McMurry, P. H., Eisele, F. L., Tanner, D. J., & Jefferson, A. (1996). MEASURED  
835 ATMOSPHERIC NEW PARTICLE FORMATION RATES: IMPLICATIONS FOR NUCLEATION  
836 MECHANISMS. *Chemical Engineering Communications*, 151(1), 53–64.  
837 <https://doi.org/10.1080/00986449608936541>
- 838 Weber, R. J., Lee, S., Chen, G., Wang, B., Kapustin, V., Moore, K., et al. (2003). New particle formation in  
839 anthropogenic plumes advecting from Asia observed during TRACE-P. *Journal of Geophysical Research:*  
840 *Atmospheres*, 108(D21). <https://doi.org/10.1029/2002JD003112>
- 841 Weigel, R., Hermann, M., Curtius, J., Voigt, C., Walter, S., Böttger, T., et al. (2009). Experimental characterization  
842 of the COndensation PArticle counting System for high altitude aircraft-borne application. *Atmospheric*

843  
844  
845  
846

*Measurement Techniques*, 2(1), 243–258. <https://doi.org/10.5194/amt-2-243-2009>  
Zelenski, M., Taran, Y., & Galle, B. (2015). High emission rate of sulfuric acid from Bezymianny volcano,  
Kamchatka. *Geophysical Research Letters*, 42(17), 7005–7013. <https://doi.org/10.1002/2015GL065340>

Accepted Article